Journal of Geochemical Exploration 186 (2018) 143–157

Contents lists available at ScienceDirect

Journal of Geochemical Exploration

journal homepage: www.elsevier.com/locate/gexplo

GEMAS: Spatial analysis of the Ni distribution on a continental-scale using digital image processing techniques on European agricultural soil data

Gyozo Jordan[a,b,*], Attila Petrik[c,**], Benedetto De Vivo[c], Stefano Albanese[c], Alecos Demetriades[d], Martiya Sadeghi[e], The GEMAS Project Team[1]

[a] Department of Applied Chemistry, Szent István University, Villányi út 35-43, 1118 Budapest, Hungary
[b] State Key Laboratory for Environmental Geochemistry, China Academy of Sciences, 550081, 99 Linchengxi Road, Guiyang, Guizhou, China
[c] Dipartimento di Scienze della Terra Università di Napoli Federico II, Via Cintia snc., 80126 Naples, Italy
[d] Institute of Geology and Mineral Exploration, Hellas
[e] Geological Survey of Sweden, Uppsala, Sweden

ARTICLE INFO

Keywords:
Univariate statistics
Numerical differential calculation
Spatial pattern
Lineament analysis
Lithology
Soil parent material

ABSTRACT

This study demonstrates the use of digital image processing for the spatial pattern recognition and characterisation of Ni concentrations in topsoil in Europe. Moving average smoothing was applied to the TIN-interpolated grid model to suppress small irregularities. Digital image processing was applied then to the grid. Several NE-SW, E-W and NW-SE oriented features were revealed at the continental scale. The dominant NE-SW linear features follow the Variscan and Alpine orogenies. The highest variability zones are in the Alps and the Balkans where mafic and ultramafic rocks outcrop. A single major E-W oriented north-facing feature runs along the last continental glaciation zone. This zone also coincides with a series of local maxima in Ni concentration along the glaciofluvial deposits. The NW-SE elongated features are located in the Pyrenees, northern Italy, Hellas and Fennoscandia. This study demonstrates the advantages of digital image processing analysis in identifying and characterising spatial geochemical patterns unseen before on conventional colour-surface maps.

1. Introduction

The Geochemical Mapping of Agricultural and Grazing Land Soil (GEMAS) project was established in 2008 as a joint project of the Geochemistry Expert Group of EuroGeoSurveys and Eurometaux (European Association of Metals) (Reimann et al., 2014a, 2014b). The project aimed at providing harmonised geochemical background data according to the specifications of the new European Chemicals Regulation, known as REACH (Registration, Evaluation and Authorisation of Chemicals; EC, 2006). In this framework, 2108 samples of agricultural soil (Ap, 0–20 cm, regularly ploughed fields), and 2023 samples from land under permanent grass cover (Gr, 0–10 cm, grazing land soil) were collected across almost the whole European continent, at an average density of 1 sample site/2500 km^2, in accordance with a commonly agreed sampling protocol (EuroGeoSurveys Geochemistry Working Group, 2009). The spatial distribution of chemical elements in the GEMAS database has been investigated by several studies using interpolated concentration maps and geostatistical analysis in order to identify anomalous patterns in relation to bedrock geology and anthropogenic contamination sources (Reimann et al., 2012; Tarvainen et al., 2013; Fabian et al., 2014; Reimann et al., 2014a, 2014b; Albanese et al., 2015; Birke et al., 2014, 2017).

In general, spatial geochemical data have long been analysed with various graphical techniques, such as proportional dots (Björklund and Gustavsson, 1987), and statistical methods, namely classification based on percentiles, boxplots (Kürzl, 1988; O'Connor and Reimann, 1993) and cumulative probability (CP) and empirical cumulative distribution function (ECDF) plots (Tennant and White, 1959; Lepeltier, 1969; Sinclair, 1974, 1976, 1983, 1986, 1991). Element concentration maps in regular grid are constructed with interpolation methods, such as polynomials functions

---

[*] Correspondence to: G. Jordan, Department of Applied Chemistry, Szent István University, Villányi út 35-43, 1118 Budapest, Hungary.
[**] Corresponding author.
E-mail address: gyozojordan@gmail.com (G. Jordan).
[1] The GEMAS Project Team: M. Andersson, R. Baritz, M.J. Batista, A. Bel-lan, M. Birke, D. Cicchella, W. De Vos, E. Dinelli, M. Ďuriš, A. Dusza-Dobek, O.A. Eggen, M. Eklund, V. Ernstsen, P. Filzmoser, D.M.A. Flight, S. Forrester, M. Fuchs, U. Fügedi, A. Gilucis, M. Gosar, V. Gregorauskiene, W. De Groot, A. Gulan, J. Halamić, E. Haslinger, P. Hayoz, R. Hoffmann, J. Hoogewerff, H. Hrvatovic, S. Husnjak, L. Janik, M. Kaminari, J. Kirby, V. Klos, F. Krone, P. Kwecko, L. Kuti, A. Ladenberger, A. Lima, J. Locutura, P. Lucivjansky, A. Mann, D. Mackovych, M. McLaughlin, B.I. Malyuk, R. Maquil, R.G. Meuli, G. Mol, P. Négrel, P. O'Connor, K. Oorts, R.T. Ottesen, A. Pasieczna, V. Petersell, S. Pfleiderer, M. Poňavič, C. Prazeres, U. Rauch, S. Radusinović, C. Reimann, I. Salpeteur, R. Scanlon, A. Schedl, A. Scheib, I. Schoeters, E. Sellersjö, I. Slaninka, J.M. Soriano-Disla, A. Šorša, R. Svrkota, T. Stafilov, T. Tarvainen, V. Trendavilov, P. Valera, V. Verougstraete, D. Vidojević and Z. Zomeni.

https://doi.org/10.1016/j.gexplo.2017.11.011
Received 12 August 2017; Received in revised form 6 November 2017; Accepted 21 November 2017

0375-6742/

over irregularly spaced data (Akima, 1996) or with kriging based on semi-variogram models (Reimann et al., 2012; Gosar et al., 2016; Birke et al., 2017). The advanced method of multi-fractal mapping has been widely used to decompose spatial geochemical data into anomalies and background values (Agterberg, 2001; Cheng et al., 1994; Cheng, 1999a, 1999b; Lima et al., 2003; Zuo et al., 2015; Zuo and Wang, 2016). Additional methods are the spatially weighted singularity mapping (Xiao et al., 2017) or the spatially weighted principal component analysis for multi-element geochemical data (Cheng et al., 2011). Local neighbourhood analysis (LNA) is another widely-used method to characterise spatial geochemical patterns (Zhang et al., 2007; Cheng, 2007; Carranza, 2009; Xie et al., 2008; Zuo, 2014). Shahi et al. (2015) proposed the coupling of discrete wavelet transforms (DWT) and principal component analysis (PCA) for predicting mineralisation. Apart from a few early attempts of digital image processing of geochemical maps, such as the pioneering work by Chork and Cruikshank (1984), no systematic application of digital image processing has been applied to spatial geochemical data, despite the extensive mapping and map interpretation in applied geochemical surveys.

Geochemical maps interpolated from the original sampling points to a regular grid can be viewed as raster images and, hence, processed using digital image processing procedures to increase the apparent distinction between spatial features. There are two basic types of procedures, global and local operations. Global operations (also called point operations) act on the whole image, on all the pixels at the same time, and modify each pixel value independently from its neighbouring pixels. Local operations (also called spatial operations), on the contrary, modify each pixel value based on the neighbouring pixel values. Global operations use the image histogram and have basically two applications. Histogram or density slicing is used to classify data based on frequency distribution characteristics (Lillesand et al., 2015). Slicing of an image histogram by dividing pixel values (element concentrations in the case of geochemical maps) into specified intervals is used in the present study to display discrete categories of element concentrations, such as anomalous and background values. Contrast stretching methods (often called normalisation) enhance image contrast by expanding the range of grey levels (colours) assigned to image pixel values. These two techniques are often used in combination where grey levels of values within a class, such as the low concentration geochemical background, are streached (also called level slicing or piecewise linear contrast stretching) in order to reveal subtle concentration patterns on the geochemical map. However, contrast enhancement should be applied only after error treatment to avoid 'over-contrasting' by assigning different display values to pixels differing only within the error range.

Local operations, also called neighbourhood operations, change a particular pixel value based on the surrounding pixel values. The 'surrounding' or neighbourhood is defined by a rectangular grid (matrix; also called window or kernel) of pixels centred over the target pixel, which is slid from pixel to pixel to make the same calculation for each pixel on the image, hence the name 'moving window' operations. The size of the moving window is defined by the number of rows and columns of the constituting pixels, such as 3 × 3 or 9 × 9 window-size, for example. Local operations include the important class of the so called 'low pass' and 'high pass' filters, besides the many and diverse procedures. Low pass filters allow the low frequency features, such as a large area of geochemical anomalies to 'pass' or remain in the image, and they filter out or remove the high frequency components, such as random noise. One of the most frequently used and simplest low pass filter is the moving average filter that calculates the average value within a moving kernel and replaces the original value of the centre pixel with the calculated window average. Average filters are used to reduce noise and smooth small irregularities that can reveal broad, regional trends. High pass filters, on the contrary, allow the high frequency features, such as sudden changes in concentration values to pass or remain in the image and they remove the low frequency components, such as the spatial trend. One of the most frequently used and simplest high pass filter is the gradient filter that calculates the concentration change from pixel to pixel.

Digital image processing is only a sub-area of the broad field of mathematics called signal processing. In this study, only a few specific signal processing procedures are used, such as the digital identification of local extreme values (minima and maxima) in the Ni concentration geochemical map, local variability characterisation (relief calculation) and auto-correlation (variogram) analysis. Finally, an interesting aspect of the digital image processing of an interpolated raster geochemical map is considering the raster map as a continuous surface of a bivariate function, much like the digital terrain model of the topographical surface. Hence, the geochemical maps can be analysed for 'slope', i.e., the rate of concentration change (gradient) or for 'aspect', i.e., the direction of the maximum change to see, for example, if the regional change of concentration has a certain geographical orientation (Jordan, 2007; Jordan et al., 2005).

The objective of this study is to demonstrate the use of digital image processing techniques for reproducible spatial geochemical pattern recognition and quantitative spatial feature characterisation. The concentrations of Ni in samples of agricultural topsoil from the GEMAS project database (Reimann et al., 2014a) are used as an example to perform the detailed spatial analysis, and to relate the spatial features to possible underlying geological and geochemical processes.

2. Materials and methods

2.1. Soil sampling and sample preparation

In the GEMAS project, a squared sampling grid of 50 × 50 km was virtually superimposed on the European continent, and the national sampling teams were free to decide where to collect the agricultural (Ap) and grazing land (Gr) soil samples across the area of 2500 km^2 of each cell. The coordinates of samples are in Lambert-Azimuthal Equal Area Projection (European Terrestrial Reference System; ETRS89) and all interpolated maps used this coordinate system. In accordance with the agreed field manual (EuroGeoSurveys Geochemistry Working Group, 2009), the agricultural soil samples were collected from regularly ploughed fields at a depth interval of 0 to 20 cm. At each sampling location, a composite sample of 3.5 kg average weight was made by mixing equal aliquots from 5 sub-sites collected from the corners and centre of a 10 × 10 m square. For quality control purposes, a field duplicate was taken at every 20th sample site with an offset distance of ca. 10–20 m from the original sampling site.

All samples were prepared in a central laboratory (Geological Survey of the Slovak Republic) (Mackových and Lučivjamský, 2014). The samples were air dried, disaggregated in a porcelain mortar and sieved to pass a 2 mm nylon screen, and finally split into sub-samples. Ten splits of < 2 mm were prepared from each sample, 4 splits of 200 ml for storage, 2 splits of 100 ml, and 4 splits of 50 ml for distribution to laboratories performing various tasks (Mackových and Lučivjamský, 2014). All samples were then randomised and analytical duplicates and project standards were introduced at a rate of 1 in 20.

2.2. Sample analysis and quality control

Nickel was among the elements determined by both X-ray fluorescence (XRF) and inductively coupled plasma-mass spectrometry after hot aqua regia extraction (AR/ICP-MS) at the laboratory of the Federal Institute for Geosciences and Natural Resources in Germany and ACME laboratories (now Bureau Veritas Minerals) in Vancouver (Canada), respectively. The aqua regia results were selected for this study because of the lower detection limit (AR/ICP-MS = 0.1 mg Ni/kg; XRF = 3 mg Ni/kg). A detailed description of the analytical methods and quality control results is provided by Reimann et al. (2009), Birke et al. (2014), and Demetriades et al. (2014). The laboratory detection limit (DL) of Ni achieved by AR/ICP-MS was low enough (0.1 mg/kg) to measure concentrations in $> 99\%$ of the Ap soil samples. While the precision at the 95% confidence level was about 6% for Ni, and the geochemical (natural), sampling (site) and analytical variance were

99.2%, 0.6% and 0.2%, respectively (Reimann et al., 2009; Demetriades et al., 2014). The overall expanded measurement uncertainty (Ramsey, 1998) for each sample site at the 95% confidence level with three measurements of the unbalanced analysis of variance design is ± 8.95%. Hence, Ni is a very suitable element for the detailed analysis of its spatial characteristics.

2.3. Data preparation

Prior to the spatial analysis of Ni concentration in agricultural topsoil, locations far from the main body of sample points, such as small distant islands, had to be excluded in order to avoid incorporating distant measurement sites into the interpolation and into spatial pattern analysis. Islands, such as the Aegean Sea islands located up to 9.3 km from the European mainland (a natural break-point on the cumulative frequency curve of the closest distance to the European mainland polygon) and having > 1 sampling site were used in the detailed spatial analysis of this study (Fig. 1). The large lands of the United Kingdom and Ireland, having 116 and 21 sampling points and being located from the larger European landmass by only 33 and 21 km, respectively, were included in the analysis. On the contrary, the islands of Cyprus, Crete and Sardinia having only 5, 5 and 10 sampling points and being located from the European mainland by the large distances of 787, 95 and 191 km, respectively, were excluded from the analysis; similarly, the one sampling point on Santa Cruz de Tenerife (Canary Islands) at a distance of > 1300 km from Europe was excluded. In total, 2032 samples were taken into consideration out of the total number of 2108 agricultural soil samples collected (Table 1, Fig. 2A).

Summary statistics used in this study include measures of central tendency and variability, i.e., minimum, lower quartile, median, upper quartile, maximum and, median absolute deviation (MAD), (Table 1). Tukey's inner-fence criteria (Tukey, 1977) were used for outlier (anomalous Ni concentration) definition (Fig. 2B). Nickel concentrations below the detection limit of 0.1 mg/kg were set to half this value for data processing. Nickel concentrations measured in soil samples on different rock types were also compared by box-and-whisker plots (Kürzl, 1988) ordered by increasing median values (Fig. 3). Nickel concentrations were classified according to the percentiles (minimum, P5, P25, P75, P90, maximum) to study their statistical distribution (Fig. 4A).

Spatial analysis in this study is based on a continuous Ni concentration surface interpolated from the 2032 sampling points using the Triangular Irregular Network (TIN) interpolation method (Guibas and Stolfi, 1985). TIN is a linear and reliable interpolation method (fits to the original data points), which does not require preliminary structural analysis, unlike kriging, and it represents the modelled surface fairly well, especially in the case of regularly located data points (Davis, 2011). Thus, TIN is a simple and satisfactory exploratory interpolation method that justifies its use in this study. Since the objective of this paper is to analyse regional-scale spatial patterns, the statistically defined boxplot outliers (Fig. 2B) are excluded before the interpolation, i.e., samples with Ni values ≥ 56.46 mg/kg (N = 115), leaving 1917 data points that were used for the final interpolation and successive analyses. Although the sampling density is 1 site/2500 km^2, the shortest distance between sampling points in neighbouring cells is 370 m. However, the TIN is resampled to a 10 × 10 km grid. This cell size is smaller than 99.3% of distances between sampling points considered in this study compromising between highest possible spatial resolution and computation efficiency, and it was used to generate the final raster map, which is the subject of further digital image processing.

Successive moving average smoothing was applied to generalise the TIN model in order to suppress small singular features and to enhance large-scale significant patterns of Ni concentration distribution in the study area. First, a series of 30 × 30, 50 × 50, 70 × 70, 90 × 90, 110 × 110, 130 × 130, 150 × 150, 170 × 170 and 210 × 210 km window-size moving average low-pass filter smoothing was applied to the original 10 km spaced TIN raster map. The TIN raster map, smoothed with the (110 × 110 km) window size, revealed best the large-scale spatial trends and patterns, without losing much detail, and it was used for digital image processing, such as edge detection, and for other analyses, for example, spatial autocorrelation and directional variogram calculations. According to Evans (1972), the statistical properties of point attributes are more stable if the 2D interpolated data surface is smoothed before analysis, further supporting the use of smoothing before spatial analysis.

Error of interpolation was estimated by calculating the difference between the smoothed TIN-interpolated surface and the original outlier-free data points used for the interpolation. Results show that the applied smoothed TIN interpolation is a good model as the error of interpolation (residuals, i.e., the difference between the interpolation surface and the measured values at the sampling points) has a symmetrical distribution, a mean equal to zero at the 95% confidence level according to the *t*-test, and the error is uncorrelated as shown by the nugget-effect variogram.

A systematic digital image processing methodology is applied to the image segmentation and image enhancement of the smoothed TIN-interpolated Ni concentration raster map according to Evans (1972) method as extended by Jordan et al. (2005) and Jordan (2007). This method, originally developed for digital elevation models, proceeds from simple univariate data display and evaluation, through edge detection and image segmentation, to the multivariate interpretation of results using GIS technology.

To begin with, the investigated smoothed TIN-interpolated outlier-free Ni map is displayed as a shaded relief surface (Fig. 5A) for visual pattern recognition. Hill shading methods producing relief maps are peculiar to raster

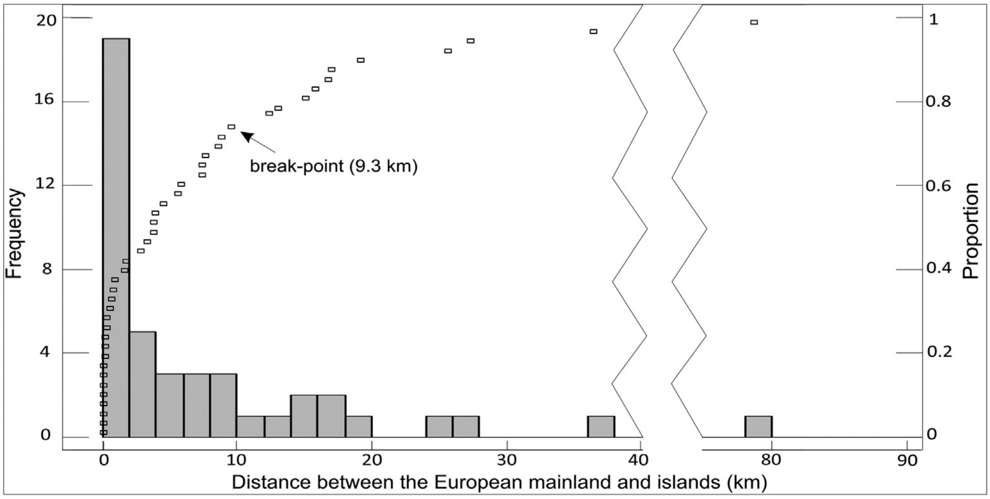

Fig. 1. Histogram and cumulative frequency distribution of distance between European mainland and islands. Note the distinct break-point on the cumulative curve at 9.3 km.

digital surface models and are fundamental for surface analysis (Simpson and Anders, 1992). In relief maps, surface features at right angle to the direction of illumination will be enhanced, while features parallel to the direction of illumination or falling in shaded areas will be seen as faint structures. Changing the lighting directions facilitates the recognition of structures in other orientations. The introduction of vertical exaggeration can be very helpful in studying minor changes in flat basin areas. Hill shading increases the contrast of very subtle intensity variations of an image, much more than contouring or pseudo-colour representation does (Burrough, 1986; Drury, 1987). In this study, the shaded relief model was overlain by local maxima and minima points extracted from the Ni concentration raster map (Fig. 5A) in order to observe their possible alignment and spatial trend in the study area. Eight shaded relief models were calculated at an azimuth interval of 45° and constant insolation inclination of 45° (Appendix SM1 in the Supplementary material). The models used the Lambertian reflection method and ten-times vertical exaggeration (Li et al., 2004).

Four digital cross-sections across the study area are shown in Fig. 5B and C running in directions perpendicular to the main spatial features, such as regional anomaly zones in order to study the local conditions at prominent features.

Terrain Ruggedness Index (TRI) proved to be an efficient tool to reveal the spatially changing variability (also called ‘heteroscedasticity’) of Ni concentration (Fig. 6A, B). TRI was calculated as the difference between the central pixel value and the mean of its neighbouring pixels for the whole map in a moving window. The window-size was increased and the 110 × 110 km window-size proved to be the most suitable to recognise areas with low and high variability in Ni topsoil concentration.

Empirical directional variograms (Cressie, 1993) were also calculated to capture anisotropy in Ni concentration in the study area (Fig. 7 and Appendix SM2 in the Supplementary material).

Singular points are identified, such as local minima, maxima and flats, which correspond to low and high Ni concentration anomalies and uniform ‘horizontal’ homogeneous concentration areas, respectively (Jordan, 2007). The localisation of surface-specific points, i.e., local maxima (peaks), minima (pits), saddle points (passes), flats and slope-breaks is fundamental in digital spatial analysis (Peucker and Douglas, 1975; Takahashi et al., 1995; Jordan, 2007). Peaks and pits were calculated using simple ‘higher than’ algorithms (Garbrecht and Martz, 1995).

The interpolated geochemical map of Ni concentration is a raster map of a continuous surface of a bivariate function, much like the digital terrain model of the topographic surface. Hence, the geochemical map can be analysed for ‘slope’, i.e., the rate of concentration change (gradient) or for ‘aspect’, i.e., the direction of the maximum change to see, for example, if the regional change of concentration has a certain geographical orientation (Jordan, 2007). The digital model of Ni concentration generated by interpolation can be regarded as a $z = f(x,y)$ bivariate function and, hence, analysed by means of differential geometry (Jordan, 2007). Introducing the following notations (after Mitasova and Hofierka, 1993) and assuming that the continuous second-order partial derivatives of the function f exist:

$$fx = \frac{\partial z}{\partial x}, fy = \frac{\partial z}{\partial y}, fxx = \frac{\partial^2 z}{\partial x^2}, fyy = \frac{\partial^2 z}{\partial y^2}, fxy = \frac{\partial^2 z}{\partial x \partial y}$$

and

$$p = f^2x + f^2y, \quad q = p + 1$$

The magnitude of the gradient vector ($\nabla f = \mathbf{grad}\,(fx, fy)$) is $|\mathrm{grad}| = \sqrt[2]{f^2x + f^2y}$ from which the steepest slope angle is computed as:

$$\gamma = arctan\sqrt{p},$$

and aspect is given by

$$\alpha = 180^\circ - arctan\left(\frac{fy}{fx}\right) + 90\left(\frac{fx}{|fx|}\right),$$

where azimuth is in degrees and measured clockwise from north. Profile curvature (curvature of normal plane section in gradient direction, k_p) is defined as:

$$k\mathrm{p} = \frac{fxxf^2x + 2\,fxy\,fx\,fy + fyy\,f^2y}{p\sqrt{q^3}}.$$

The gradient magnitude (‘slope’) and direction (‘aspect’) were calculated to capture the maximum change of Ni concentration and its direction (see Figs. 8 and 9). Large slope values with homogeneous gradient direction along linear features may indicate geological influence on chemical element concentrations. Profile curvature, which is the 2nd derivative in the gradient direction, was used to identify areas with sudden Ni concentration changes and inflection lines between convex and concave areas (Fig. 10). If these lines are linear, they may suggest geological or tectonic control on the spatial pattern of Ni concentration in European topsoil. The calculation of the necessary first-order derivatives (fx, fy) used the unweighted eight-point numerical differentiation method (Prewitt operators) for its smoothing effect. Prewitt operators are high-pass gradient filters that calculate the partial derivatives in the x and y axes directions in a 3 × 3 moving window (Gonzalez and Woods, 1993). The second-order derivatives (fxx, fyy, fxy) used the scheme of the ILWIS 3.8[2] software. In order to improve classification of gradient direction (aspect) data based on the histogram, the aspect histogram curves were smoothed with 5RSSH five-point median filter to remove the systematic error shown as peaks at values of 45° azimuth due to numerical derivation over a rectangular grid (Jordan, 2003). The 5RSSH filter calculates the median of the five successive data points in the moving window and then applies a linear smoothing to the thus obtained median data series, which is finally corrected for possible errors at the two edges of the smoothed median data series (Tukey, 1977).

Sub-population identification followed the ‘natural break’ histogram slicing method (Abdaal et al., 2013). A natural break is defined in the cumulative distribution function (CDF) at an inflection point identified visually on the cumulative distribution function curve. This point corresponds to a local minimum in the frequency histogram (multi-modal histogram, see Fig. 9C). The identified classes of the mapped Ni concentration are displayed as homogeneous areas in the classified Ni concentration maps (Figs. 9A, B and 10).

Significant linear features, associated with sudden changes on the Ni concentration map, defined by sharp grey-scale edges in the processed digital maps, such as the shaded relief model or sharp boundaries in the classified parameter maps, for example, the slope, aspect and profile curvature maps, were digitised on screen. A lineament density map was also plotted by calculating the total length of lineaments within an aggregation window (Silverman, 1986). Several window-sizes from 10 × 10 to 500 × 500 km were tested to find the optimum solution between noise removal and keeping information detail. The 100 × 100 km window size delivered the most spatial information in this case. The obtained lineament density map was smoothed using a 110 × 110 km simple moving average filter to increase visual interpretability (Fig. 11A). Frequency and length-based directional rose diagrams from the digitised lineaments were made to see their orientation distribution.

Finally, verification of digital spatial data processing and data analysis results was carried out and all the above obtained Ni concentration maps were compared to parent material associations (Hartwich et al., 2005), lithological (Dürr et al., 2005) and Quaternary glaciation maps (Anderson and Borns, 1997; Spielhagen et al., 2004; Svendsen et al., 2004; Plant et al., 2003, 2005) using GIS overlays. Spatial modelling was performed with Golden Software's Surfer 10,[3] ILWIS 3.8 and ArcGIS 10.0[4] software.

---

[2] http://52north.org/communities/ilwis/ilwis-open.

[3] http://52north.org/communities/ilwis/ilwis-open.

[4] http://resources.arcgis.com/en/help/main/10.0/index.html.

3. Results

3.1. Statistical analysis

According to the empirical histogram and cumulative frequency plot, the Ni data (N = 1917) have a homogeneous unimodal right-skewed distribution with 115 high-outliers (≥ 56.46 mg/kg) based on Tukey's inner-fence criteria (Fig. 2). The Ni concentrations in the data set (N = 2032) used in this study vary from < 0.1 (0.05) to 2475 mg/kg, with a median value of 14.6 mg/kg and a median absolute deviation (MAD) of 9.13 mg/kg (34% relative variability) (Table 1).

Out of the 2032 sampling points, 1699 sites were assigned to 8 main bedrock types, based on the lithological map in Fig. 4B, and the corresponding Ni concentrations were displayed in box-and-whiskers plots in the order of increasing median values (Fig. 3). It is noted that the remaining 333 sampling sites were over undifferentiated parent materials (e.g., alluvial, deluvial or glacial drift sediments). Ultramafic rocks have the highest median Ni concentration value (83.9 mg/kg), which is followed by volcanoclastic (36.3 mg/kg), siliciclastic (20.2 mg/kg), carbonate (19.3 mg/kg), metamorphic (14.9 mg/kg), mafic (14.5 mg/kg), felsic (9.3 mg/kg), intermediate (8.2 mg/kg) and undifferentiated (6.6 mg/kg) rocks. According to the Mann-Whitney test (Mann and

Table 1
Statistical parameters of Ni in agricultural soil for the whole data set, and the subset used in this study, with the percentage proportion of samples below the detection limit (DL).

Data set	N	DL	Min	P10	P25	P50	P75	P90	Max	MAD	Mean	SD	IQR	Range
Full	2032	0.1	< **0.1**	3.1	6.7	**14.6**	26.6	41.4	**2475**	9.14	25.6	75.4	19.9	2475
Outlier-free	1917	0.1	< **0.1**	2.9	6.3	**13.6**	23.9	34.6	**56.3**	8.33	16.5	12.3	17.6	56.3

Full: data set without the sample points in the excluded islands. Outlier-free: data set without the islands and the high outliers. Min and Max: minimum and maximum values, respectively. P: percentiles. Note that P50 is the meadian. MAD: median absolute deviation. SD: standard deviation. IQR: inter-quartile range. Emboldened numbers emphasise the minimum, maximum and median. Values are given in unis of mg/kg. See text for details.

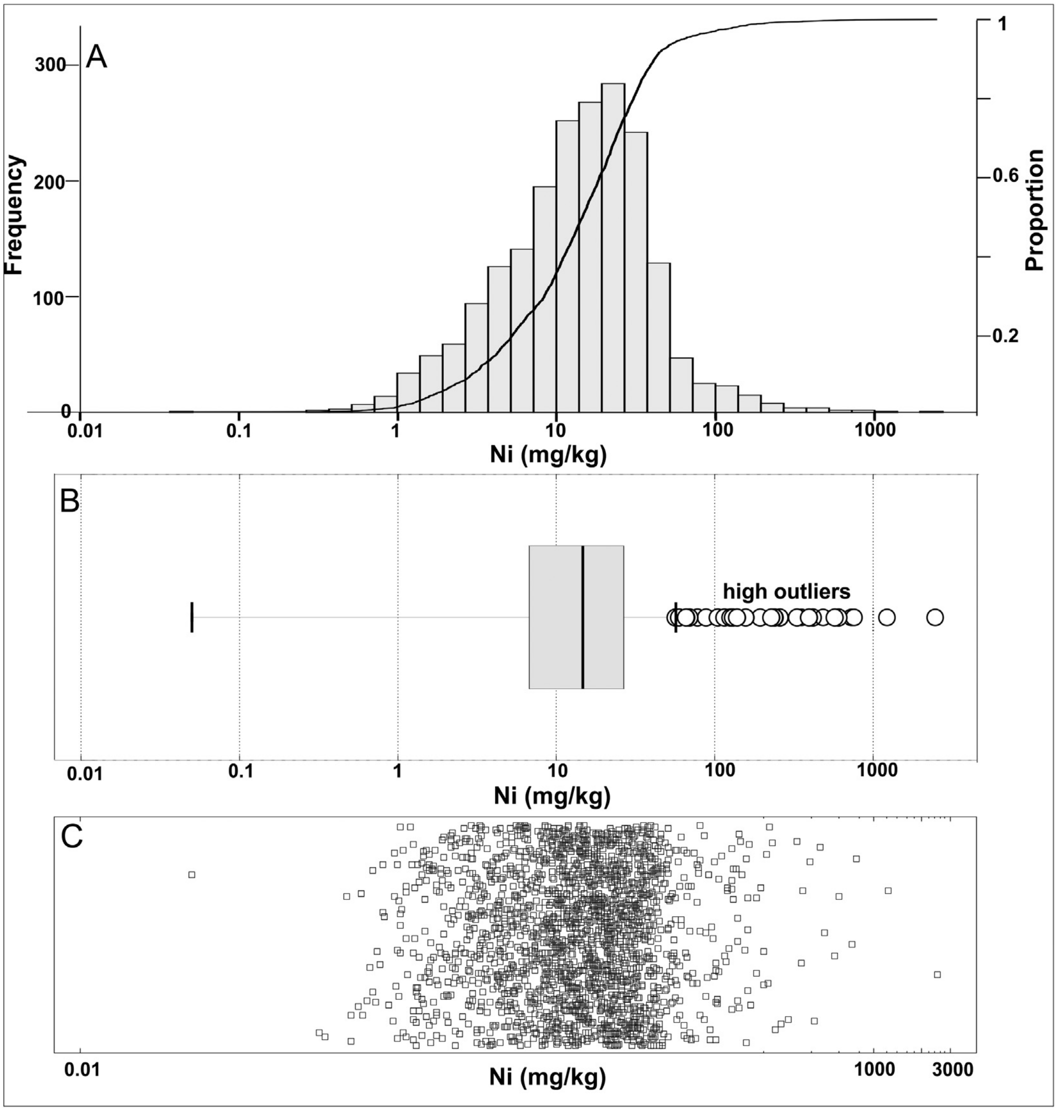

Fig. 2. Statistical univariate distribution analysis of Ni (Ap). A. Empirical histogram with the cumulative frequency distribution curve. B. Boxplot showing univariate outliers. C. Two-dimensional scatterplot. Note the log-scale of x-axis on the plots.

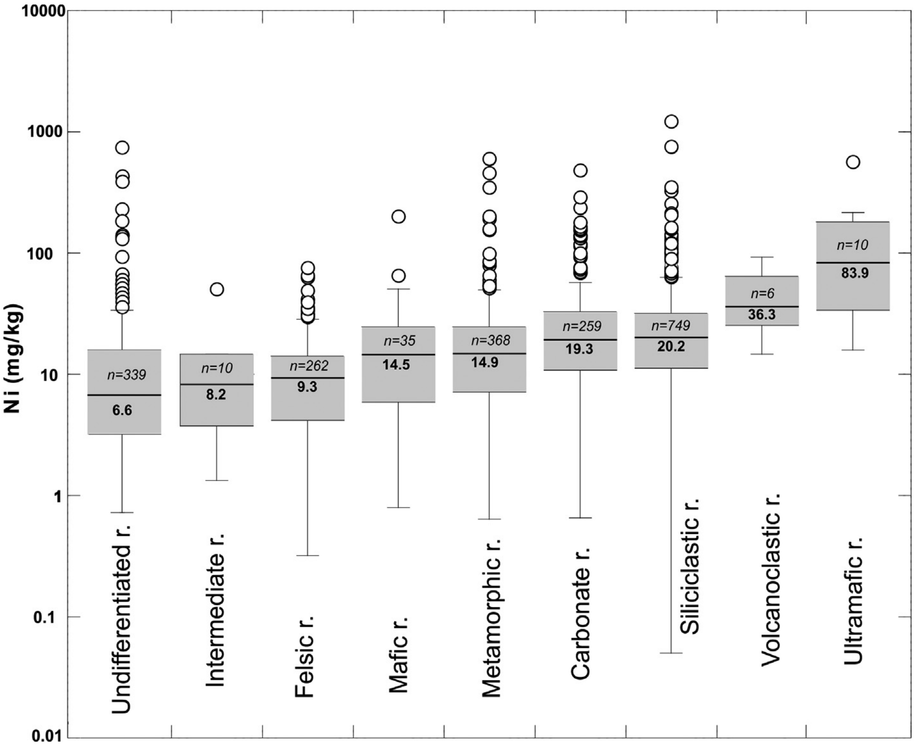

Fig. 3. Box-and-whisker plot of Ni concentrations in topsoil samples calculated for different bedrock parent materials, arranged in increasing order of median values. Bold numbers in the boxes indicate the median value of the correspondent group; n indicates the number of samples in the corresponding group. Note that volcanoclastic rocks have only 6 samples, intermediate rocks and ultramafic rocks have only 10 samples each.

Whitney, 1947), 4 groups can be distinguished based on the homogeneity of the median values at the 95% confidence level. The 1st group refers to topsoil samples over undifferentiated, felsic and intermediate rocks, the second includes mafic and metamorphic rocks parent materials, the 3rd carbonate and siliciclastic rocks and the 4th group only ultramafic rocks. Topsoil over volcanoclastic rocks has only 6 samples, which is insufficient for the Mann-Whitney test (a minimum of 8 samples is required).

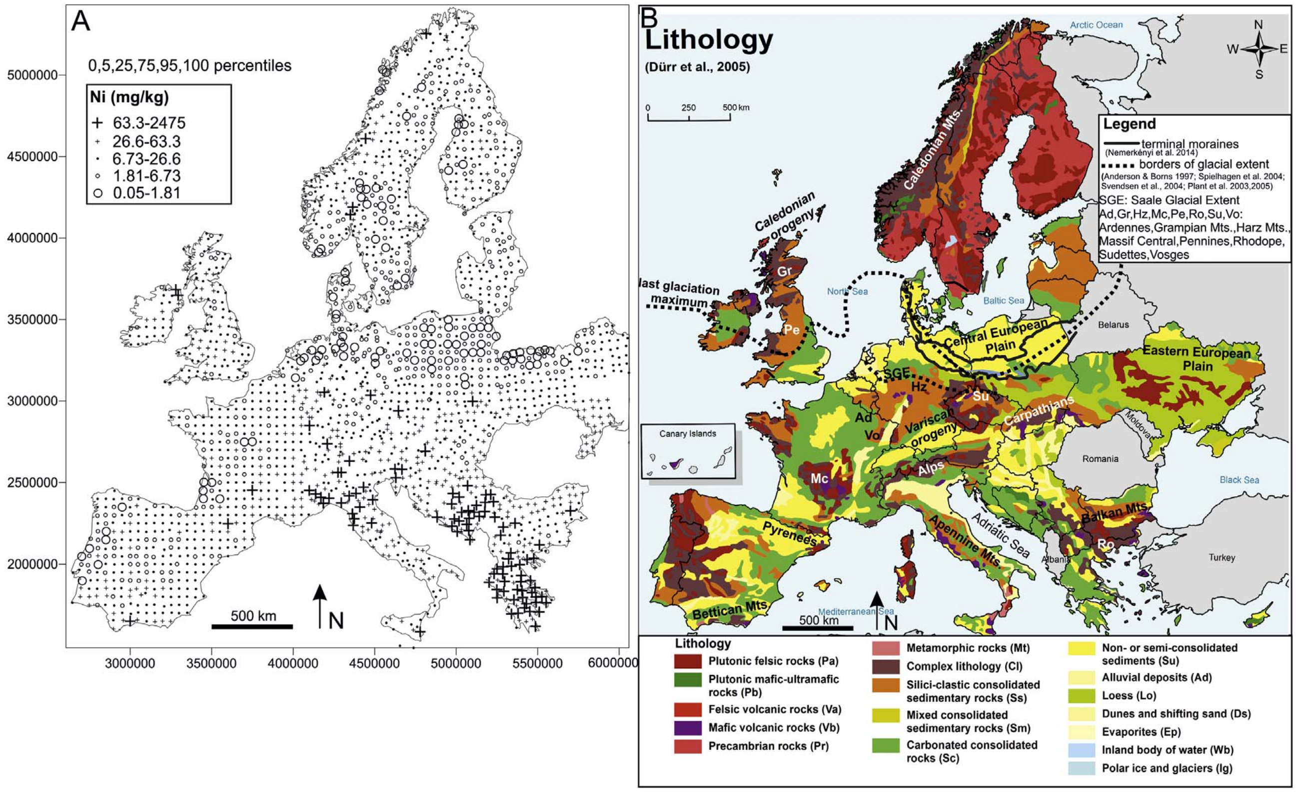

Fig. 4. A. Ni concentrations map based on EDA percentiles symbols (N = 2032). B. Lithology map of Europe (modified after Dürr et al., 2005). Note that low Ni concentrations are located along the E-W zone of the last continental glacial maximum and terminal moraines. The highest Ni concentrations are observed in the Balkan Peninsula and northern Italy where mafic and ultramafic rocks outcrop, as well as rocks derived from them. (For interpretation of the references to colour in this figure legend, the reader is referred to the web version of this article.)

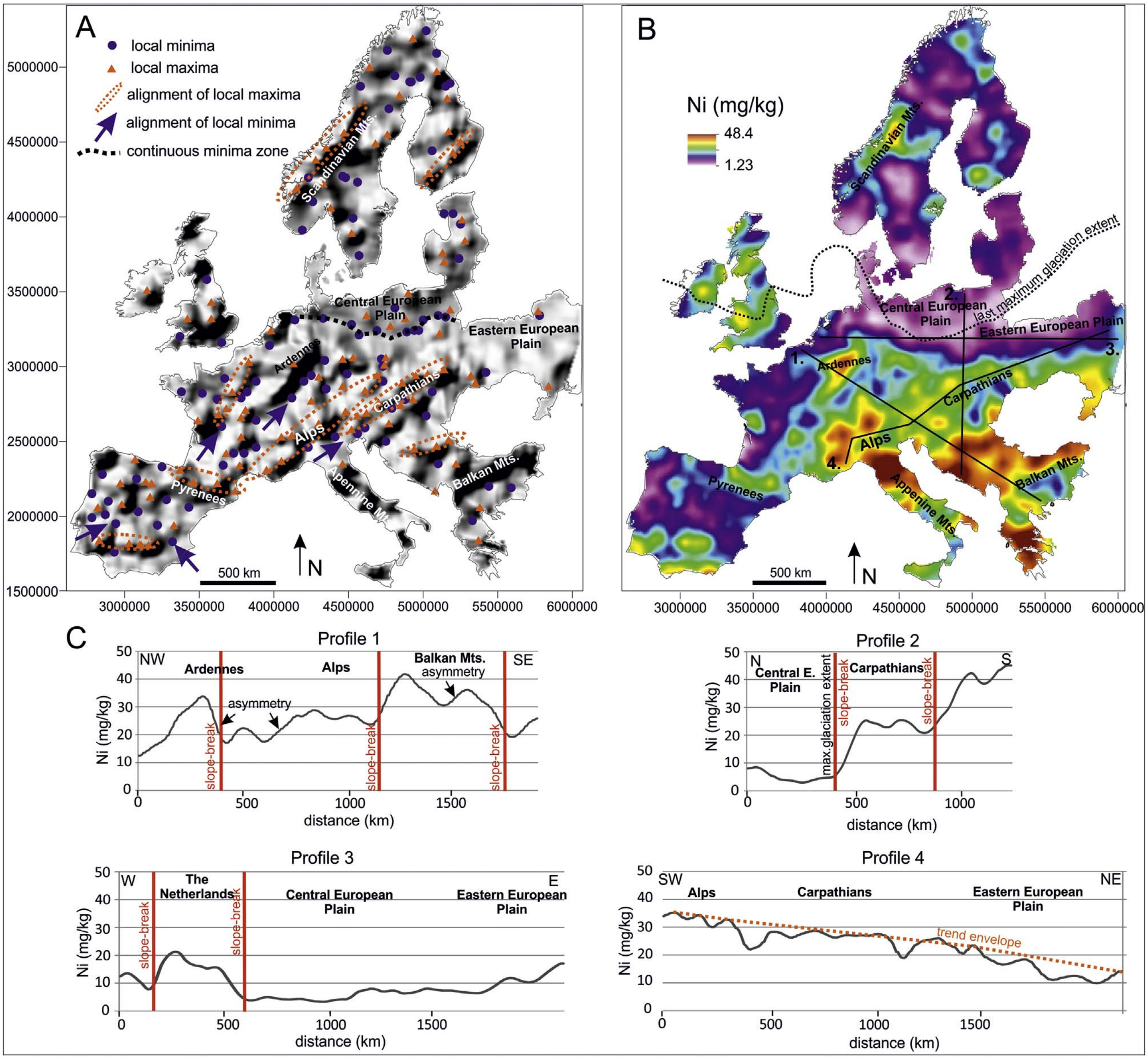

Fig. 5. A. Shaded relief map of the outlier-free Ni data overlain by the local maxima and minima points. Note their dominating NE-SW alignments emphasised by blue arrows and orange dashed ellipsoids. B. TIN-interpolated Ni concentrations map with traces of cross-sections shown below. The main Ni relief regions are also indicated. C. Cross-sections of Ni concentrations made perpendicular and parallel to the main spatial features. Large slope-breaks are shown with thick red lines and trend envelope with orange dashed line. (For interpretation of the references to colour in this figure legend, the reader is referred to the web version of this article.)

3.2. Mapping and spatial analysis

The Ni concentration map, classified by using EDA percentiles, reveals that the majority of low concentration samples (< 1.81 mg/kg, 5% percentile) are concentrated in an E-W trending zone in the northern part of the Central European mainland (Fig. 4A), covering approximately the Central European Plain, which is delineated by the limit of the last continental glaciation and terminal moraines to the south (Fig. 4B). A NE-SW oriented low Ni value zone is located in the western part of the Iberian Peninsula, where felsic rocks are dominant. Other low Ni value sample sites occur in the Aquitaine and Paris Basins in France with mudstone, siltstone, sandstone and carbonate lithologies, and are more randomly distributed in Fennoscandia over felsic (igneous and metamorphic) rocks (Fig. 4A) (Jähne, 2014). The high Ni values (> 63.3 mg/kg, 95th percentile) are clustered in the Balkan Peninsula, and in the northern part of Italy in the Alps and Apennine Mts, where mafic and ultramafic rocks outcrop as well as rocks derived from them (Figs. 4A, B and 5B). It is worth noting that these zones of high Ni values have a dominant NE-SW orientation.

The shaded relief model of the smoothed TIN-interpolated raster map reveals several regional linear features of locally high Ni values oriented in the NE-SW direction across the whole study area (Fig. 5A). These zones are more easily seen on the TIN interpolated map in Fig. 5B. More interesting is that the digitally identified local minima and maxima points align in the same NE-SW direction (Fig. 5A). These sub-parallel NE-SW oriented zones are hundreds of kilometres long and some of them follow the strike of large mountain chains, such as the Alps, the Carpathians and the Scandinavian/Fennoscandian Mts. A local NW-SE trending maxima zone is also identified in the Iberian Peninsula, which runs parallel to the strike of the Pyrenees (Fig. 5A). A further interesting feature is the roughly E-W oriented continuous undulating line composed of several local minima points along the southern border of the Central European Plain running sub-parallel to the southern limit of the last maximum continental glaciation extent (Fig. 5A, B).

The NW-SE oriented cross-section, calculated from the smoothed TIN Ni concentration raster map, running across the centre of the study

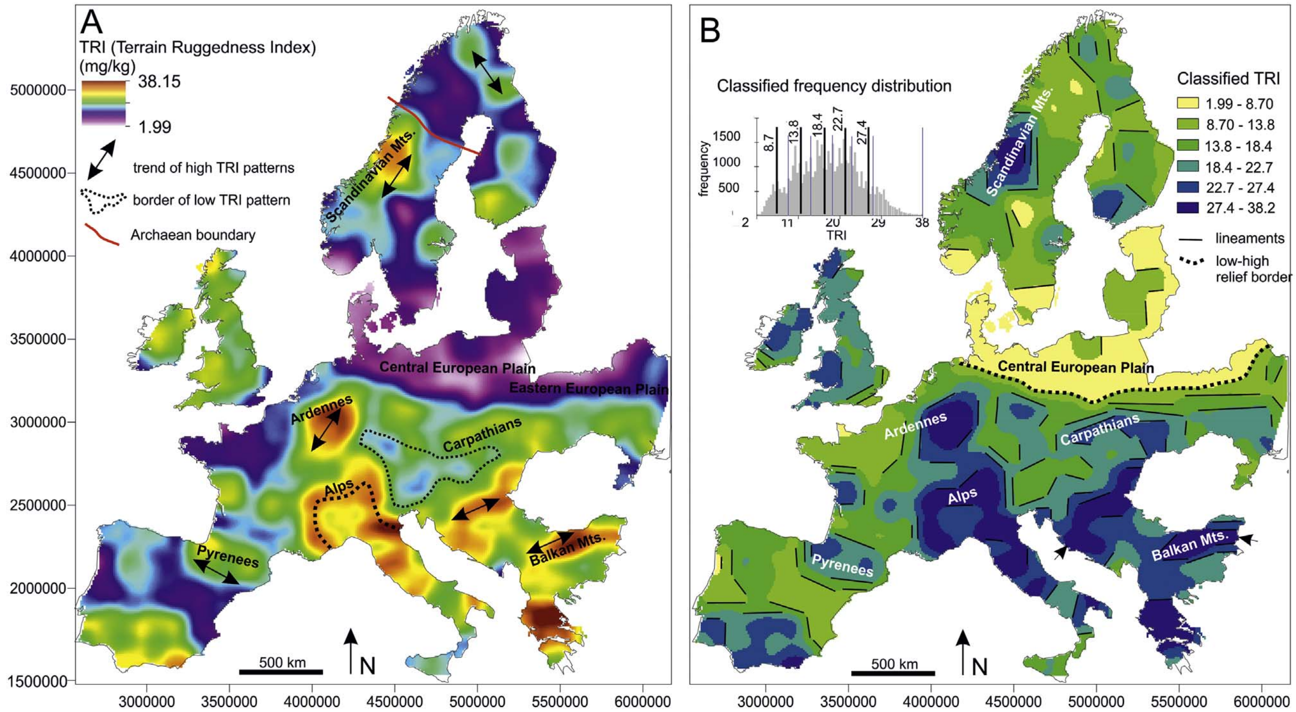

Fig. 6. A. Terrain Ruggedness Index (TRI) map of outlier-free Ni values. Note the NE-SW oriented high heteroscedasticity zones. Also note the roughly E-W border along the Central European Plain which separates low and high variability zones. B. Classified TRI map based on histogram slicing. Note the linear edges of the different variability zones. (For intepretation of the references to colour in this figure legend, the reader is referred to the web version of this article.)

area, transects the elongated NE-SW zones and displays abrupt changes in Ni concentration (Fig. 5C, Profile 1). The NE-SW trending high Ni concentration zones appear as peaks at prominent mountains, such as the Ardennes and Balkan Mts., having asymmetric shape and bordered by large slope-breaks where Ni concentrations increase abruptly. Profile 4 in Fig. 5C, along the prevailing NE-SW oriented high Ni concentration zones, clearly shows a steadily decreasing trend from the SW to the NE from the Alps to the Carpathians and the Eastern European Plain. The N-S oriented profile reveals abrupt increase of Ni concentrations with significant slope-breaks south of the last continental glaciation zone (Fig. 5B, C, Profile 2). The E-W oriented profile uncovers a large depression zone of Ni values, which roughly coincides with the area of the Central European Plain (Fig. 5B, C, Profile 3).

The Terrain Ruggedness Index (TRI) map, calculated with a 110 × 110 km moving window from the outlier-free smoothed TIN surface, was enhanced for visual interpretation by post-processing with a 110 × 110 km moving average smooth (Fig. 6A, B). The most prominent feature is the large area of low variability in the northern part of the Central European mainland. A sharp, undulating and several hundreds of kilometres long, roughly E-W oriented line is apparent, which separates the high and low variability zones along the southern border of the Central and Eastern European Plain (Fig. 6A), which coincides with the southern limit of the last continental glaciation. A distinct NW-SE line in northern Scandinavia coincides with the Archaean and Palaeo-Proterozoic rocks contact, called the Archaean Boundary. The highest variability zones (TRI = 27–38), running in an overall NE-SW direction from the Scandinavian Mts to the Balkan Mts, including the Ardennes, Alps and Carpathians, are discernible on the TRI map

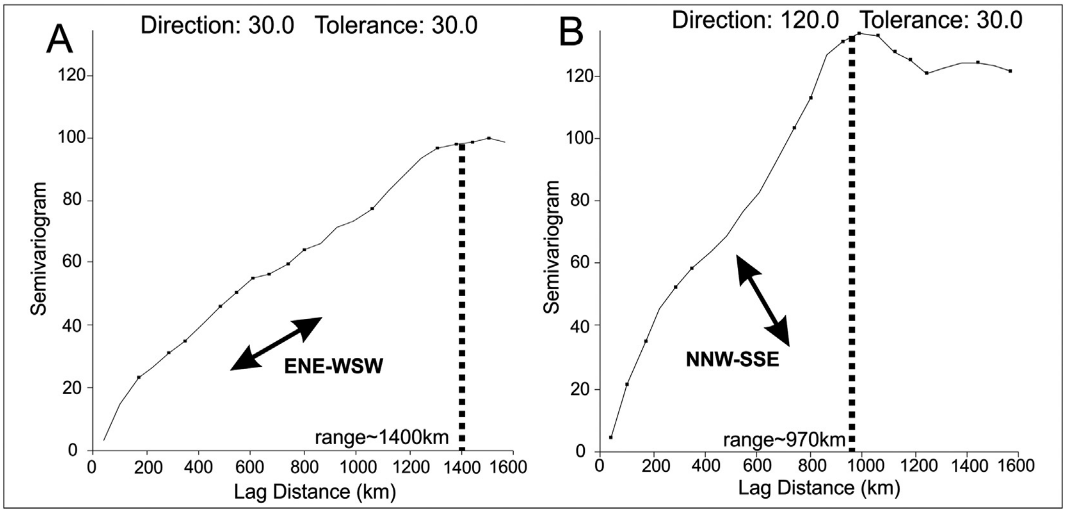

Fig. 7. Directional semi-variograms in (A) ENE-WSW and (B) NNW-SSE direction. Note the longer range in the ENE-WSW direction. The averaged semi-variogram values are displayed on the y-axis.

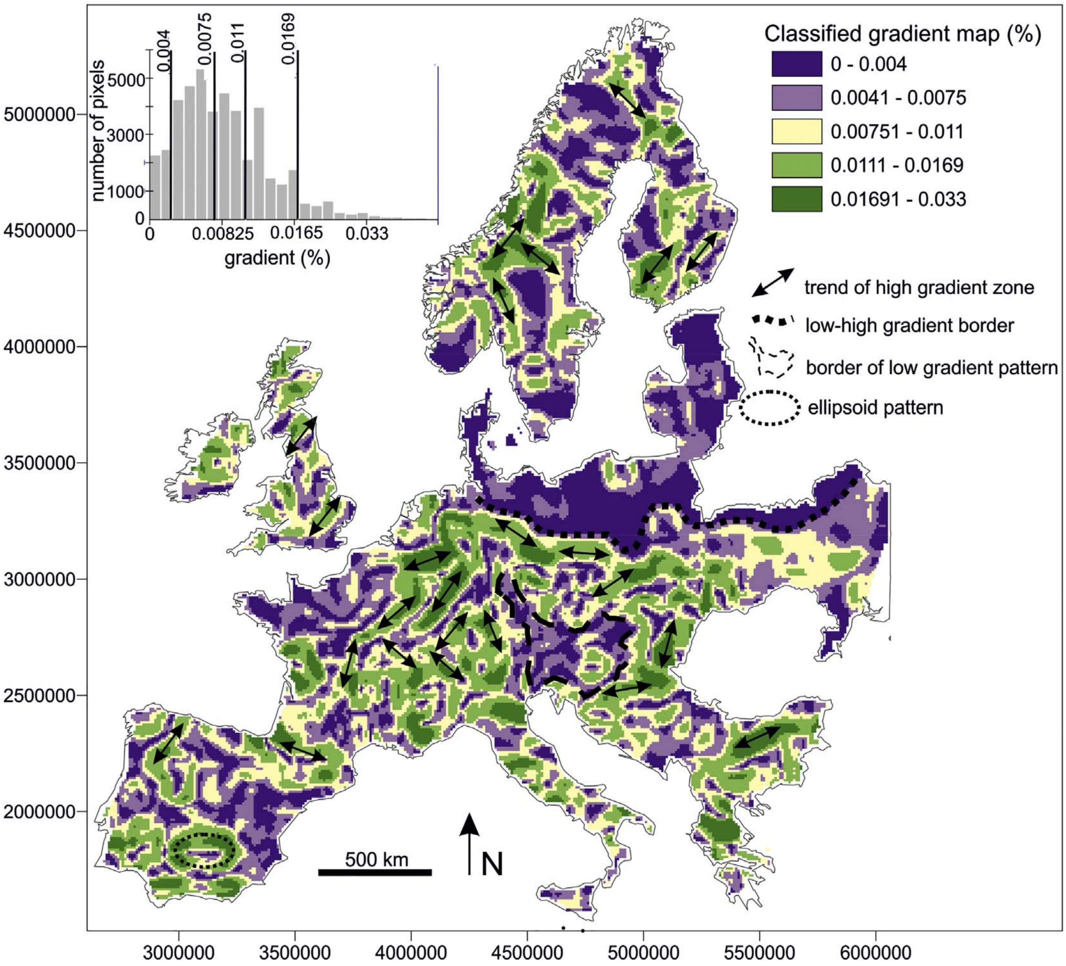

Fig. 8. Classified gradient map calculated from the smoothed TIN Ni concentrations map showing the NE-SW, NW-SE and E-W orientation of elongated linear patterns (emphasised by black arrows), and the continuous border between high and low gradient zones in northern Central Europe (shown by black dotted line), which coincides with the southern limit of the last continental glaciation. The histogram displays the classes based on natural break-points. (For interpretation of the references to colour in this figure legend, the reader is referred to the web version of this article.)

(Fig. 6A). A moderate variability area (TRI = 13–18) in the centre of Europe is encircled by the above mentioned high value zones (Fig. 6A). The classified TRI map uncovers that the high variability areas are mainly located in the Fennoscandian/Scandinavian Mts., Apennines, Carpathians and the Balkan Peninsula with several NE-SW oriented features (see dark blue areas in Fig. 6B). A NW-SE oriented high variability zone along the Pyrenees is also displayed. It is interesting that the areas with different variability often have sharp linear edges (Fig. 6B).

A strong ENE-WSW trending anisotropy in the correlation of Ni concentrations, elongated parallel to the alignment of local maxima and minima points, is captured by the directional semi-variograms (Fig. 7A, B). The range in the ENE-WSW direction is about 1400 km, while it is only 970 km in the perpendicular NNW-SSE direction.

The classified gradient magnitude (in percentage slope) map shows the magnitude of Ni topsoil concentration change in the gradient vector direction. High values indicate a large change with respect to unit distance (Fig. 8). The highest gradient magnitude areas have elongated shape in the prevailing NE-SW direction. Occasionally, like in Fennoscandia, northern Italy and Hellas, NW-SE elongated features are apparent, too. Uniform Ni concentration values are shown as low gradient areas in Fig. 8, again most notably in the area of the Central and Eastern European Plain.

The classified gradient direction (aspect) map overlain by the local minima and maxima points is shown in Fig. 9A. Fig. 9B emphasises the sharp edges as lineaments between areas of homogeneous gradient direction value. The histogram of the gradient direction ranging from 0° to 360° displays significant multi-modality (peaks) corresponding to pixels facing the same direction (Fig. 9C). The classified gradient direction map is characterised by the cross-cutting NE-SW oriented zones, which are hundreds of kilometres long and are bounded by sharp linear edges. Some perpendicular short, NW-SE oriented features are located inside the main NE-SW trending zones. North-west to south-east oriented long features are also discernible in the Iberian Peninsula and Fennoscandia, northern Italy and northern Hellas. An obvious feature is that the local minima and maxima points perfectly align, along the sharp borders of the main features (Fig. 9A). The most striking pattern is, however, the extensive E-W oriented north facing homogenous zone extending from the English Channel to the Eastern European Plain (Fig. 9A, B). The N-S digital cross-section across this zone also shows the decreasing Ni concentration in the northerly direction in this area (Fig. 5C, Profile 2). Its southern and northern borders are marked by a series of local maxima and minima, respectively. In this homogeneous Ni concentration area the prevailing NE-SW elongated trans-continental zones are disrupted and absent (Fig. 9A, B). The rose diagram of the lineaments (Fig. 9D), digitised from the Fig. 9B map, displays the main directions.

The second derivative of Ni concentration, calculated in the gradient direction, is the profile curvature and it shows the change in the gradient magnitude (slope) (Fig. 10). The profile curvature map is classified according to its sliced histogram of the outlier-free data set. In this figure, the NE-SW oriented main linear zones clearly emerge as

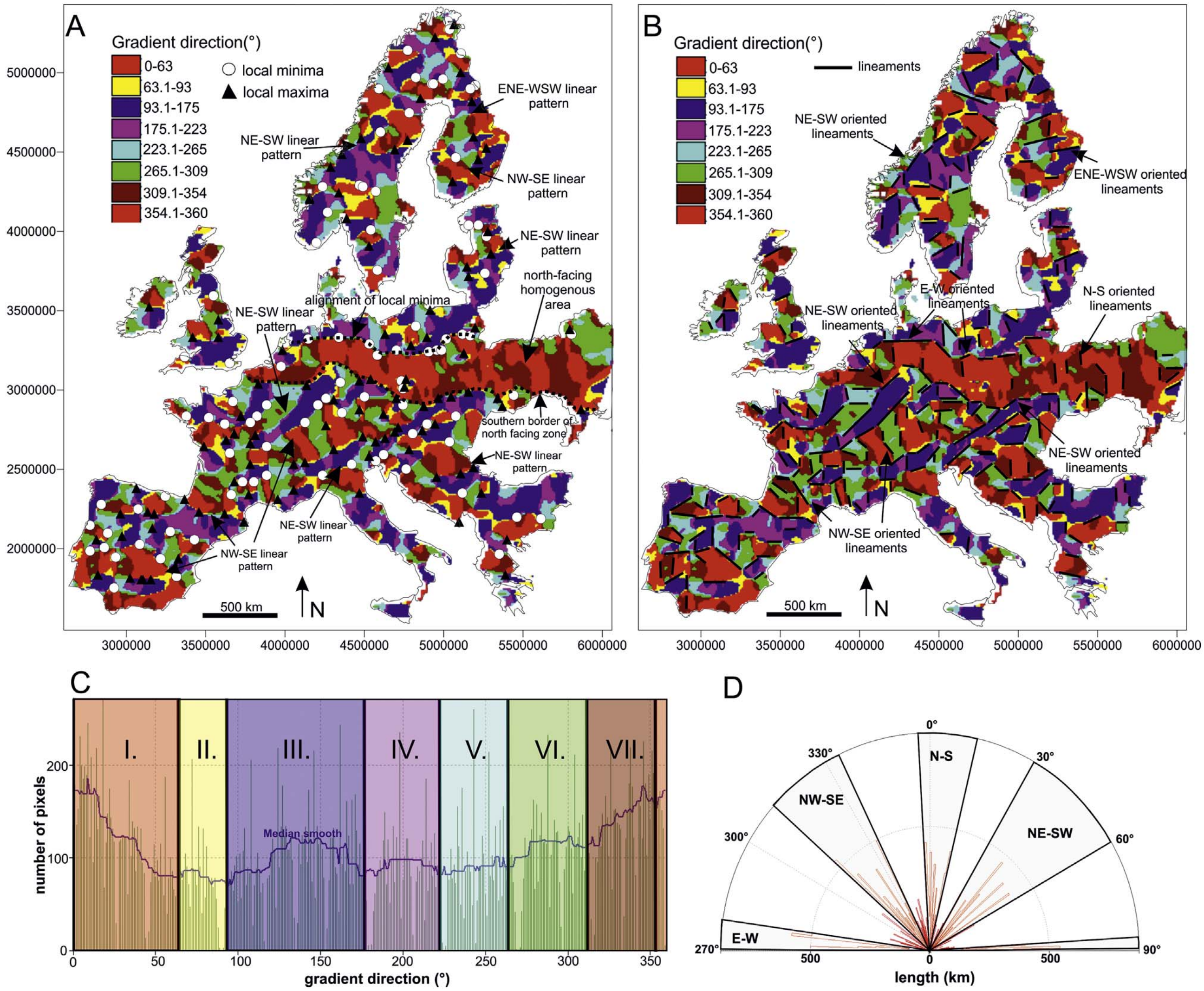

Fig. 9. A. Classified gradient direction map overlain by the local maxima and minima points. Note the coincidence of the alignment of these extreme points with NE-SW, NW-SE and E-W oriented linear patterns. B. Classified gradient direction map overlain by lineaments digitised from the classified aspect map. The linear edges of different gradient direction zones can be seen. C. Frequency distribution of gradient direction smoothed by 5 × 5 5RSSH median filter developed by Tukey (1977) (blue line). The classes were identified by histogram-slicing based on natural break-points. D. Length-based direction distribution of lineaments. Note the 4 major orientations corresponding to the main linear patterns. (For interpretation of the references to colour in this figure legend, the reader is referred to the web version of this article.)

distinct features with many high negative (convex; solid black lines in Fig. 10) and positive (concave; dashed black lines in Fig. 10) curvature values. These patterns are sub-parallel and abrupt, marked by an E-W oriented, hundreds of kilometres long wavy slope-break zone (heavy dotted line) in the northern part of Central Europe. Besides the prevailing NE-SW oriented areas, convex and concave zones elongated in the NW-SE direction are also identified in the Iberian Peninsula, Fennoscandia and the British Islands, but are not very discernible in northern Italy and Hellas. Some ellipsoid shaped convex features can be recognised in the southern part of the Iberian Peninsula and Sweden (Fig. 10).

All significant linear edges on the previous maps were manually digitised as lineaments. The lineament density map shows that linear edges are focused in the main NE-SW trending zones (Fig. 11A). The sharp E-W running boundary in northern Central Europe is obvious on this map, and separates low and high lineament density zones to the north and south, respectively.

According to the lineament length and frequency rose diagrams shown in Fig. 11B, there are four major directions in the spatial pattern of Ni concentrations in topsoil: NE-SW, ENE-WSW, N-S and NW-SE. The highest dispersion in the lineament orientation is associated with the NE-SW and ENE-WSW directions.

4. Discussion

By means of digital image processing applied to the GEMAS geochemical map of agricultural topsoil Ni concentrations, several spatial features have been identified and significant spatial patterns unfolded, which were not observed before on conventional colour-surface geochemical maps.

The statistical analysis of Ni concentrations in agricultural topsoil samples revealed a right-skewed unimodal distribution with 114 high-outliers, which are mainly clustered in the Balkan and Apennine Peninsulas (Fig. 4A). The highest Ni values are related to ultramafic and mafic rocks (e.g., ophiolite complexes) (Figs. 3 and 4B) where the median value is 83.9 mg/kg (Fig. 3). Low values are concentrated on the Central and Eastern European Plain, where several local minima points align along the zone of glacial sands delimited by the southernmost limit of the last continental glaciation maximum (Figs. 4A, B, 5A, B and 12).

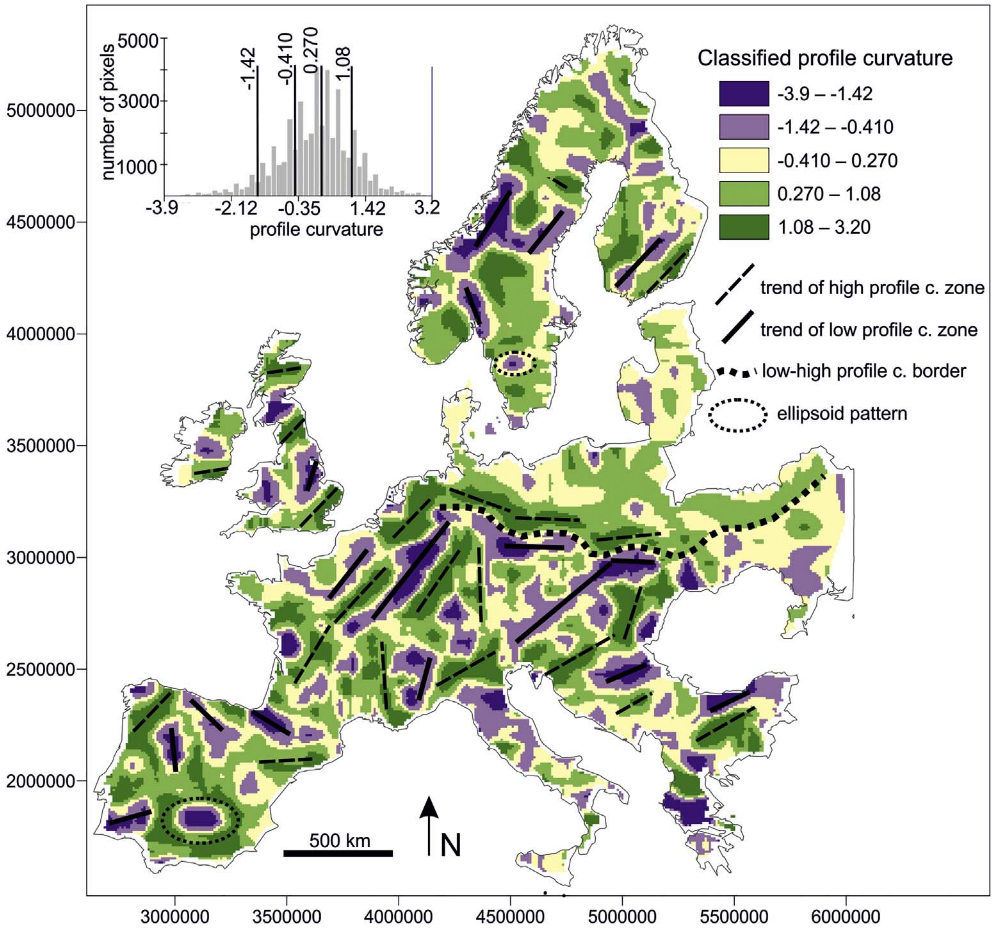

Fig. 10. Classified profile curvature map of Ni outlier-free data. Histogram displays classes by using natural-break points. Note the predominance of NE-SW trending linear patterns south of the border separating low-high profile curvature zones (marked with black dotted line). (For interpretation of the references to colour in this figure legend, the reader is referred to the web version of this article.)

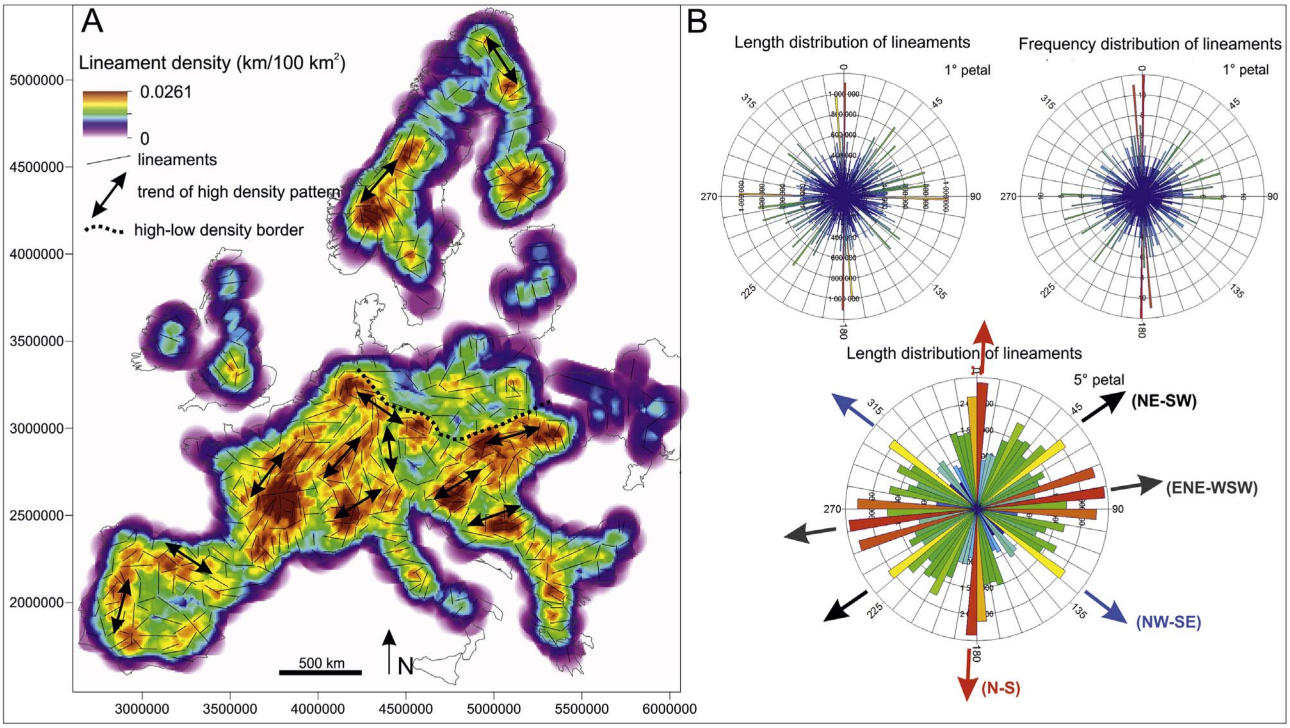

Fig. 11. A. Lineament density map with main trends of high density zones (black arrows). B. Length-based (1° and 5° petals) and frequency-based (1° petal) directional distribution of lineaments. Note the four main directions corresponding to the orientation of major linear patterns. (For interpretation of the references to colour in this figure legent, the reader is referred to the web version of this article.)

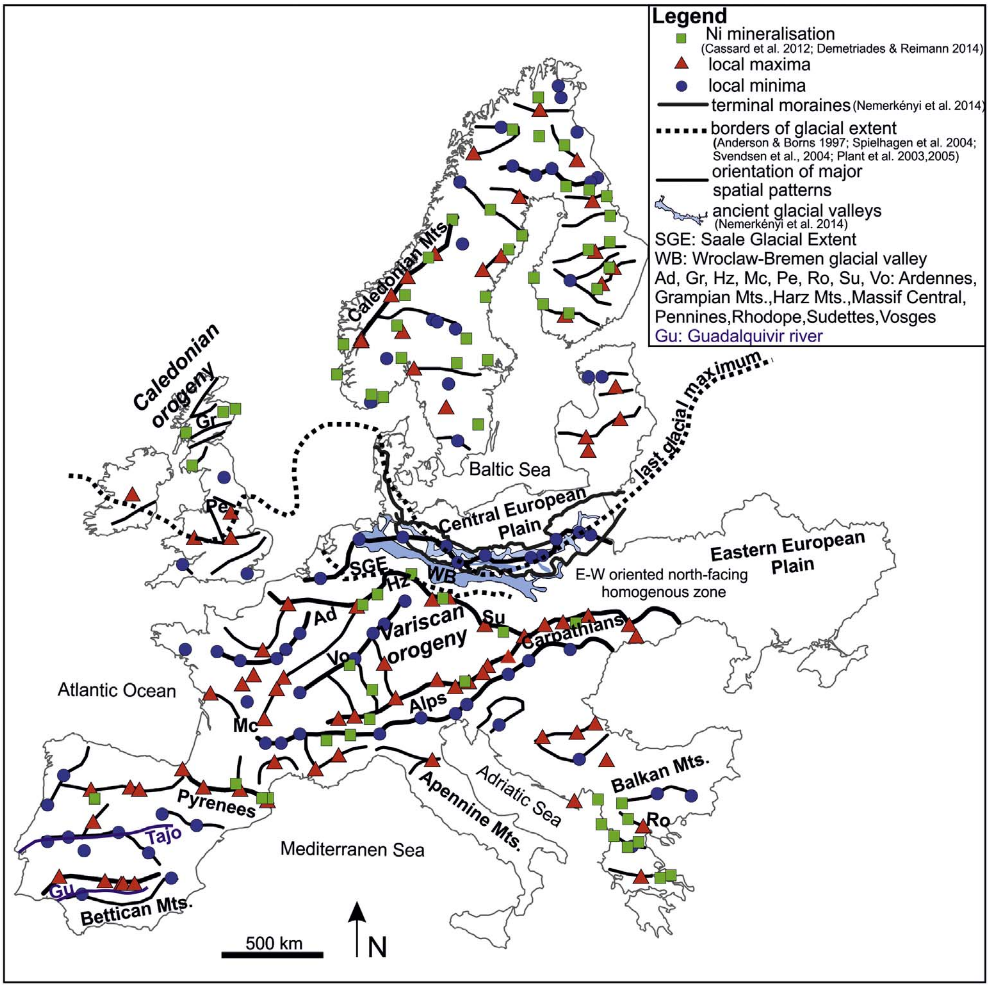

Fig. 12. The main trends of the identified spatial features along with local minima/maxima and Ni mineralisation occurrences. Limits of continental glaciation extents, ancient glacial valleys and terminal moraines are also displayed. Note the spatial coincidence between the local minima points and the last continental glaciation maximum extent and terminal moraines. Roughly E-W trending glacial valleys are sub-parallel to this minimum zone. Also note the predominance of NE-SW and ENE-WSW trending features south of the continental glaciation limits. (For interpretation of the references to colour in this figure legend, the reader is referred to the web version of this article.)

A remarkable E-W running line is revealed by most of the image processing outputs, such as the digital cross-sections, the TRI variability map, the gradient and the lineament density maps (Figs. 5, 6, 8–12). This line corresponds to the maximum extent of the last continental glaciation at the southern border of the Central European Plain. According to Salminen et al. (2005), De Vos, Tarvainen et al. (2006), Scheib et al. (2014), Reimann et al. (2014a, 2014c) and Albanese et al. (2015), across the border of the last continental glaciation the spatial distribution and concentration of chemical elements in topsoil change significantly. The lowest Ni values ($<$ 15 mg/kg) are found north of the border line where acidic soil with an average pH value of 5.66 and humid climate is prevailing (Braunschweiler and Koivisto, 2000; Salminen et al., 2005; De Vos, Tarvainen et al., 2006; Reimann et al., 2014a). In addition, the classified gradient direction (aspect), the TRI, digital cross-sections and profile curvature maps indicate that this E-W running border line is in fact a complex zone, and it is composed of many narrow sub-parallel zones across, which the Ni concentration values change abruptly (Figs. 5C, 6, 9, 10). These sub-parallel zones in the Central and Eastern European Plain coincide with E-W oriented glaciofluvial valleys and terminal moraines (e.g., Warsaw-Berlin, Wroclaw-Bremen), which evolved mainly in the Elster and Saale continental glaciation periods (Fig. 12) (Anderson and Borns, 1997; Spielhagen et al., 2004; Svendsen et al., 2004; Plant et al., 2003, 2005; Nemerkényi et al., 2014).

Further, the gradient direction (aspect) map reveals an interesting E-W oriented north-facing homogenous zone from the English Channel to the Eastern European Plain (Fig. 9A, B). Its northern border coincides with a series of local minima points running sub-parallel to the last continental glaciation maximum extent limit and the lithological border between semi-consolidated moraine and glaciofluvial sediments and carbonate rocks (Figs. 4B, 9, 12). Its southern border coincides with a series of local maxima points, which run sub-parallel to the boundary line of the Saale glaciation (Fig. 12). In addition, this southern border separates the glaciofluvial plains (e.g., Central European Plain) from the outcrops of Variscan and Alpine orogeny (e.g., Harz Mts., Ardennes, Sudetes, Carpathians), where mafic and ultramafic rocks outcrop and several Ni ore mines and prospects occur (Cassard et al., 2012; Demetriades and Reimann, 2014) (Fig. 12). The glacial area is characterised by low variability and homogeneously low topsoil Ni concentrations, which steadily decrease from south to north. This investigation also revealed that the continental glaciation boundary is composed of several sub-parallel zones with respect to Ni geochemistry.

The other main spatial patterns, the prevailing trans-continental NE-SW oriented elongated zones terminate abruptly at the above E-W running homogeneous area of the last continental glaciation (Figs. 9, 10, 12), then continue further to the north in Fennoscandia. These sub-parallel concave (low anomaly) and convex (high anomaly) geochemical zones include several aligned local minima and maxima points, respectively (Figs. 9, 10, 12). Their orientation is continuously changing in clockwise direction corresponding to the strike of major fault zones from the Atlantic Ocean to the Black Sea (Fig. 12). These NE-SW zones have large slope-breaks and are characterised by asymmetry where the Ni concentration values change abruptly (Fig. 5C, Profile 1). They run parallel to the Variscan orogeny trend including the Ardennes, Vosges, Massif Central, Harz Mts and Sudetes, while in the east and south they follow the structures of the Alpine orogeny, including the

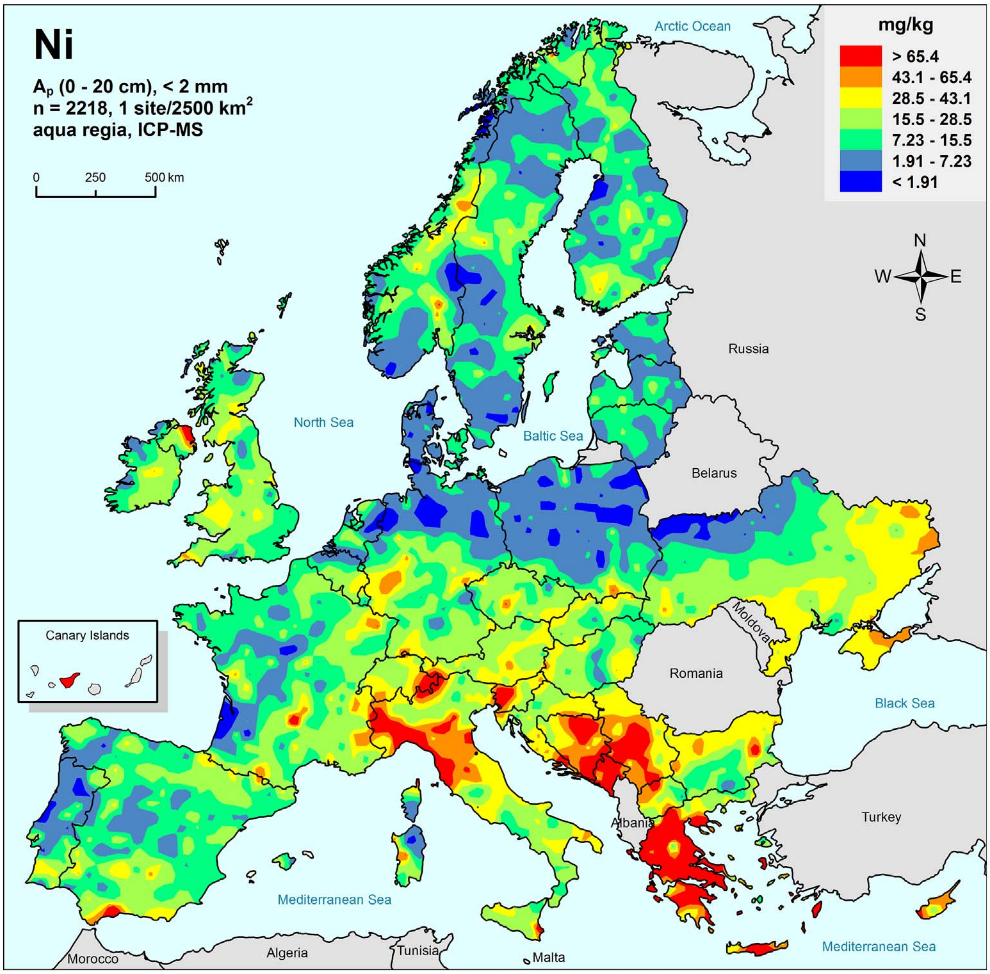

Fig. 13. Original colour-surface map of Ni concentration in agricultural topsoil map (Reimann et al., 2014a, Fig. 11.39.5, p.329). Note that the locations of high Ni values are clearly clustered in the Balkan Peninsula and in the northern part of Italy in the Alps and Apennine Mts. The zone of the last glaciation is also obviously marked by the area of low Ni values in the Central and Eastern European Plain. See text for details. (For interpretation of the references to colour in this figure legent, the reader is referred to the web version of this article.)

Alps and the Carpathians (Fig. 12).

Linear patterns with a NE-SW orientation were also identified in the greenstone belts of the Caledonian Mts, which include several local Ni maxima and mineralisation occurrences (Fig. 12). Some mineralisation sites in Scotland are located along NE-SW oriented linear features following the average strike of the Caledonian structures (Figs. 4B and 12) (Windley, 1984; McKerrow et al., 2000).

Other elongated spatial features striking WNW-ESE and WSW-ENE are alternating in the Iberian Peninsula (Fig. 12). The former is partially related to the Pyrenees where local maxima and mineralisation sites are clustered. The latter is mainly observable at the northern border of the Baetic Mountains. It is interesting to see that some local minima (e.g., Tajo River) and maxima points (e.g., Guadalquivir River) align along some major rivers of the Iberian Peninsula (Fig. 12). Some rivers might have an important role in the redistribution of chemical elements, such as Ni in agricultural soil, which in most cases is developed on alluvial deposits.

Finally, it is emphasised that the original colour-surface map of Ni concentration in agricultural topsoil in the 'Chemistry of Europe's Agricultural Soils' atlas (Fig. 13; Reimann et al., 2014a) also shows the remarkable E-W running line between low and high value areas to the north and south, respectively, which corresponds to the limit of the last continental glaciation maximum, as observed, for example, by Salminen et al. (2005), De Vos, Tarvainen et al. (2006), Scheib et al. (2014), Reimann et al. (2014c), and Albanese et al. (2015). In addition, the high Ni values clustering in the Balkan Peninsula and in the northern part of Italy (Alps and Apennine Mts) can be readily observed on the original map (Fig. 13). However, the digital image processing methods enable the reproducible delineation of these areas and the quantitative characterisation of their spatial distribution. Other patterns discussed in this paper, such the multiple boundaries of the last glaciation or the SW-NE linear features are not readily revealed by the visual study of the original colour-surface map (Fig. 13).

5. Conclusions

In this study the novel application of digital image processing methods to geochemical map analysis is described and demonstrated through the example of Ni concentrations in European agricultural topsoil. The applied systematic methodology proceeds from the simple statistical analysis to the more complex procedures, such as autocorrelation and variogram analyses. Image classification and various edge detection methods captured the same spatial patterns and identified the same features. Aspect analysis and local minima and maxima identification proved to be particularly successful in pattern recognition in this study. The applied methods identified spatial distribution patterns in Ni concentrations in agricultural soil not seen before, such as the multiple slope-break lines of the last continental glaciation and the trans-continental zones and trends. The most important advantage of the digital (numerical) image processing of geochemical maps, as compared to the traditional visual interpretation, is that this method provides reproducible and quantitative results.

Supplementary material to this article can be found online at https://doi.org/10.1016/j.gexplo.2017.11.011.

Acknowledgements

The GEMAS project is a cooperative project of the EuroGeoSurveys

Geochemistry Expert Group with a number of outside organisations (e.g., Alterra, The Netherlands; Norwegian Forest and Landscape Institute; Research Group Swiss Soil Monitoring Network, Swiss Research Station Agroscope Reckenholz-Tänikon, several Ministries of the Environment and University Departments of Geosciences, Chemistry and Mathematics in a number of European countries and New Zealand; ARCHE Consulting in Belgium; CSIRO Land and Water in Adelaide, Australia), and Eurometaux. The analytical work was co-financed by the following industry organisations: Eurometaux, European Borates Association, European Copper Institute, European Precious Metals Federation, International Antimony Association, International Lead Association-Europe, International Manganese Institute, International Molybdenum Association, International Tin Research Institute, International Zinc Association, The Cobalt Development Institute, The Nickel Institute, The (REACH) Selenium and Tellurium Consortium and The (REACH) Vanadium Consortium. The Directors of the European Geological Surveys, and the additional participating organisations, are thanked for making sampling of almost all of Europe in a tight time schedule possible. Support of the OTKA NKFIH Fund No. SNN118101 and from the European Structural and Investment Funds (grant agreement no. VEKOP-2.3.3-15-2017-00022) is acknowledged. We thank Christopher C. Johnson (United Kingdom), Simon Pirc (Slovenia) and Manfred Birke (Germany) for reviewing the original manuscript, and with their constructive comments the paper was considerably improved. The excellent research conditions and fruitful discussions provided by Professor Jiubin Chen of the State Key Laboratory for Environmental Geochemistry, China Academy of Sciences, Guiyang, China, helped improve the research and publication quality of this study. Finally, the two unknown reviewers are thanked for their constructive comments.

References

Abdaal, A., Jordan, G., Szilassi, P., 2013. Testing contamination risk assessment methods for mine waste sites. Water Air Soil Pollut. 224 (1416), 1–26. http://dx.doi.org/10.1007/s11270-012-1416-x.

Agterberg, F.P., 2001. Multifractal simulation of geochemical map patterns. In: Merriam, D.F., Davis, J.C. (Eds.), Geologic Modeling and Simulation. Computer Applications in the Earth Sciences. Springer, Boston, MA, pp. 327–346. http://dx.doi.org/10.1007/978-1-4615-1359-9_17.

Akima, H., 1996. Rectangular-grid-data surface fitting that has the accuracy of a bicubic polynomial. ACM Trans. Math. Softw. 22, 357–361.

Albanese, S., Sadeghi, M., Lima, A., Cicchella, D., Dinelli, E., Valera, P., Falconi, M., Demetriades, A., De Vivo, B., The GEMAS Project Team, 2015. GEMAS: Cobalt, Cr, Cu, and Ni distribution in agricultural and grazing land soil of Europe. In: Demetriades, A., Birke, M., Albanese, S., Schoeters, I., De Vivo, B. (Eds.), Continental, Regional and Local Scale Geochemical Mapping. Special Issue, Journal of Geochemical Exploration, vol. 154. pp. 81–93. http://dx.doi.org/10.1016/j.gexplo.2015.01.004.

Anderson, B.G., Borns, H.W., 1997. The Ice Age World. Scandinavian Univ. Press, Oslo (208 pp).

Birke, M., Reimann, C., Fabian, K., 2014. Analytical methods used in the GEMAS project. In: Reimann, C., Birke, M., Demetriades, A., Filzmoser, P., O'Connor, P. (Eds.), Chemistry of Europe's Agricultural Soils — Part A: Methodology and Interpretation of the GEMAS Data Set. Geologisches Jahrbuch (Reihe B102) Schweizerbarth, Hannover, pp. 41–46 (Chapter 5).

Birke, M., Reimann, C., Rauch, U., Ladenberger, A., Demetriades, A., Jähne-Klingberg, F., Oorts, K., Dinelli, E., Halamic, J., 2017. GEMAS: cadmium distribution and its sources in agricultural and grazing land soil of Europe- original data versus clr-transformed data. J. Geochem. Explor. 173, 13–30. http://dx.doi.org/10.1016/j.gexplo.2016.11.007.

Björklund, A., Gustavsson, N., 1987. Visualization of geochemical data on maps: new options. J. Geochem. Explor. 29, 89–103.

Braunschweiler, H., Koivisto, S., 2000. Fate and Effects of Chemicals in the Nordic Environments Related to the Use of Biocides. Nordic Council of Ministers, Copenhagen (135 pp).

Burrough, P.A., 1986. Principles of Geographic Information Systems for Land Resource Assessment. Monographs on Soil and Resources Survey No. 12. Oxford Science Publications, New York (193 pp.).

Carranza, E.J.M., 2009. Geochemical anomaly and mineral prospectivity mapping in GIS. In: Hale, M. (Ed.), Handbook of Exploration and Environmental Geochemistry. vol. 11 Elsevier, Amsterdam (368 pp).

Cassard, D., Bertrand, G., Maldan, F., Gaàl, G., Kaija, J., Aatos, S., Angel, J.M., Arvanitidis, N., Ballas, D., Billa, M., Christidis, C., Dimitrova, D., Eilu, P., Filipe, A., Gazea, E., Inverno, C., Kauniskangas, E., Maki, T., Matos, J., Meliani, M., Michael, C., Mladenova, V., Navas, J., Niedbal, M., Perantonis, G., Pyra, J., Santana, H., Serafimovski, T., Serrano, J.J., Strengell, J., Tasev, G., Tornos, F., Tudor, G., 2012. ProMine pan-European Mineral Deposit database: a new dataset for assessing primary mineral resources in Europe. In: Workshop on: Mineral Resources Potential Maps: A Tool for Discovering Future Deposits. 12th–14th March 2012, Nancy, France, Proceedings, pp. 9–13.

Cheng, Q., 1999a. Multifractal interpolation. In: Lippard, S.J., Naess, A., Sinding-Larsen, R. (Eds.), Proceedings of the Fifth Annual Conference of the International Association for Mathematical Geology, Trondheim, Norway, 6–11 Aug. 1999. Norway University of Science and Technology, Trondheim, pp. 245–250.

Cheng, Q., 1999b. Multifractality and spatial statistics. Comput. Geosci. 25, 949–961.

Cheng, Q., 2007. Mapping singularities with stream sediment geochemical data for prediction of undiscovered mineral deposits in Gejiu, Yunnan Province, China. Ore Geol. Rev. 32, 314–324.

Cheng, Q., Agterberg, F.P., Ballantyne, S.B., 1994. The separation of geochemical anomalies from background by fractal methods. J. Geochem. Explor. 51, 109–130.

Cheng, Q., Bonham-Carter, G., Wang, W., Zhang, S., Li, W., Xia, Q., 2011. A spatially weighted principal component analysis for multi-element geochemical data for mapping locations of felsic intrusions in the Gejiu mineral district of Yunnan, China. Comput. Geosci. 37, 662–669.

Chork, C.Y., Cruikshank, B.I., 1984. Statistical map analysis of regional stream sediment data from Australia. J. Geochem. Explor. 21, 405–419.

Cressie, N., 1993. Statistics for Spatial Data. J. Wiley & Sons, New York, NY (928 pp).

Davis, J.C., 2011. Statistics and Data Analysis in Geology. J. Wiley & Sons, India (656 pp).

De Vos, W., Tarvainen, T., Salminen, R., Reeder, S., De Vivo, B., Demetriades, A., Pirc, S., Batista, M.J., Marsina, K., Ottesen, R.T., O'Connor, P.J., Bidovec, M., Lima, A., Siewers, U., Smith, B., Taylor, H., Shaw, R., Salpeteur, I., Gregorauskiene, V., Halamic, J., Slaninka, I., Lax, K., Gravesen, P., Birke, M., Breward, N., Ander, E.L., Jordan, G., Duris, M., Klein, P., Locutura, J., Bellan, A., Pasieczna, A., Lis, J., Mazreku, A., Gilucis, A., Heitzmann, P., Klaver, G., Petersell, V. (Eds.), 2006. Geochemical Atlas of Europe: Part 2 - Interpretation of Geochemical Maps, Additional Tables, Figures, Maps, and Related Publications. Geological Survey of Finland, Espoo (Chief Editors). 692 pp. http://weppi.gtk.fi/publ/foregsatlas/.

Demetriades, A., Reimann, C., 2014. Mineral deposits in Europe. In: Reimann, C., Birke, M., Demetriades, A., Filzmoser, P., O'Connor, P. (Eds.), Chemistry of Europe's Agricultural Soils – Part B: General Background Information and Further Analysis of the GEMAS Data Set. Geologisches Jahrbuch (Reihe B103) Schweizerbarth, Hannover, pp. 71–78 (Chapter 3).

Demetriades, A., Reimann, C., Filzmoser, P., 2014. Evaluation of GEMAS project quality control results. In: Reimann, C., Birke, M., Demetriades, A., Filzmoser, P., O'Connor, P. (Eds.), Chemistry of Europe's Agricultural Soils – Part A: Methodology and Interpretation of the GEMAS Data Set Geologisches Jahrbuch (Reihe B102). Schweizerbarth, Hannover, pp. 47–60 (Chapter 6).

Drury, S.A., 1987. Image Interpretation in Geology. Allen and Unwin, London, pp. 290.

Dürr, H.H., Meybeck, M., Dürr, S.H., 2005. Lithologic composition of the Earth's continental surfaces derived from a new digital map emphasizing riverine material transfer. Glob. Biogeochem. Cycles 19 (4), 1–22. http://dx.doi.org/10.1029/2005GB002515/epdf.

EC, 2006. Regulation (EC) No 1907/2006 of The European Parliament and of The Council of 18 December 2006 Concerning the Registration, Evaluation, Authorisation and Restriction of Chemicals (REACH), Establishing A European Chemicals Agency, Amending Directive 1999/45/EC and Repealing Council Regulation (EEC) No 793/93 and Commission Regulation (EC) No 1488/94 As Well As Council Directive 76/769/EEC and Commission Directives 91/155/EEC, 93/67/EEC, 93/105/EC and 2000/21/EC. Off. J. Eur. Union L 396, Luxembourg. 518 pp. http://eur-lex.europa.eu/legalcontent/EN/TXT/PDF/?uri = CELEX:02006R1907-20130701&rid = 2.

EuroGeoSurveys Geochemistry Working Group, 2009. EuroGeoSurveys geochemical mapping of agricultural and grazing land soil of Europe (GEMAS): field manual. In: NGU Report 2008–038. Trondheim, Norway, Geological Survey of Norway 46 pp. http://www.ngu.no/upload/Publikasjoner/Rapporter/2008/2008_038.pdf.

Evans, I.S., 1972. General geomorphometry, derivatives of altitude, and descriptive statistics. In: Chorley, R.J. (Ed.), Spatial Analysis in Geomorphology. Methuen, London, pp. 17–90.

Fabian, C., Reimann, C., Fabian, K., Birke, M., Baritz, R., Haslinger, E., The GEMAS Project Team, 2014. GEMAS: spatial distribution of the pH European agricultural and grazing land soil. Appl. Geochem. 48, 207–216. http://dx.doi.org/10.1016/j.apgeochem.2014.07.017.

Garbrecht, J., Martz, L.W., 1995. Agricultural research service publication NAWQL 95-3. In: TOPAZ: An Automated Digital Landscape Analysis Tool for Topographic Evaluation, Drainage Identification, Watershed Segmentation and Subcatchment Parameterisation. TOPAZ User Manual U.S. Department of Agriculture (110 pp).

Gonzalez, R.C., Woods, R.E., 1993. Digital Image Processing. Pearson Prentice Hall, Upper Saddle River (943 pp).

Gosar, M., Šajn, R., Teršič, T., 2016. Distribution pattern of mercury int he Slovenian soil: geochemical mapping based on multiple geochemical datasets. J. Geochem. Explor. 167, 38–48.

Guibas, L., Stolfi, J., 1985. Primitives for the manipulation of general subdivisions and the computation of Voronoi diagrams. ACM Trans. Graph. 4 (2), 74–123.

Hartwich, R., Baritz, R., Fuchs, M., Krug, D., Thiele, S., 2005. Explanation to the Soil Regions Map of the European Union and Adjacent Countries 1:5,000,000 (Version 2.0). European Soil Bureau, research reports, Luxemburg.

Jähne, F., 2014. Geology of Europe. In: Reimann, C., Birke, M., Demetriades, A., Filzmozer, P., O'Connor, P. (Eds.), Chemistry of Europe's Agricultural Soils – Part B: General Background Information and Further Analysis of the GEMAS Data Set. Geologisches Jahrbuch (Reihe B 103) Schweizerbarth, Hannover, pp. 47–70 (Chapter 2).

Jordan, G., 2003. Morphometric analysis and tectonic interpretation of digital terrain data: a case study. Earth Surf. Process. Landf. 28, 807–822.

Jordan, G., 2007. Digital terrain analysis in a GIS environment. Concepts and development. In: Peckham, R.J., Jordan, G. (Eds.), Digital Terrain Modelling, Development and Applications in a Policy Support Environment. Springer Verlag, Berlin, pp. 2–39.

Jordan, G., Meijninger, B.M.L., van Hinsbergen, D.J.J., Meulenkamp, J.E., van Dijk, P.M., 2005. Extraction of morphotectonic features from DEMs: development and applications for study areas in Hungary and NW Greece. Int. J. Appl. Earth Obs. Geoinf. 7, 163–182.

Kürzl, H., 1988. Exploratory data analysis: recent advances for the interpretation of geochemical data. J. Geochem. Explor. 30, 309–322.

Lepeltier, C., 1969. A simplified statistical treatment of geochemical data by graphical representation. Econ. Geol. 64 (5), 538–550.

Li, Z., Zhu, C., Gold, C., 2004. Digital Terrain Modeling: Principles and Methodology. CRC Press (340 pp).

Lillesand, T., Kiefer, R.W., Chipman, J., 2015. Remote Sensing and Image Interpretation. Wiley Inc. (736 pp).

Lima, A., De, Vivo B., Cicchella, D., Cortini, M., Albanese, S., 2003. Multifractal IDW interpolation and fractal filtering method in environmental studies: an application on regional stream sediments of (Italy), Campania region. Appl. Geochem. 18, 1853–1865.

Mackových, D., Lučivjamský, P., 2014. Preparation of GEMAS project samples and standards. In: Reimann, C., Birke, M., Demetriades, A., Filzmoser, P., O'Connor, P. (Eds.), Chemistry of Europe's Agricultural Soils – Part A: Methodology and Interpretation of the GEMAS Data Set. Geologisches Jahrbuch (Reihe B102) Schweizerbarth, Hannover, pp. 37–40 (Chapter 4).

Mann, H.B., Whitney, D.R., 1947. On a test of whether one of two random variables is stochastically larger than the other. Ann. Math. Stat. 18 (1), 50–60.

McKerrow, W.S., Niocaill, C.Mac, Dewey, J.F., 2000. The Caledonian orogeny redefined. J. Geol. Soc. 157, 1149–1154.

Mitasova, H., Hofierka, J., 1993. Interpolation by regularised spline with tension: II. Application to terrain modelling and surface geometry analysis. Math. Geol. 25, 655–657.

Nemerkényi, A., Horváth, G., Simon, D., 2014. The central European plain. In: Gábris, Gy (Ed.), The Regional Physical Geography of Europe. Elte, Eötvös Kiadó, Budapest, pp. 77–83 (In Hungarian).

O'Connor, P.J., Reimann, C., 1993. Multielement regional geochemical reconnaissance as an aid to target selection in Irish Caledonian terrains. J. Geochem. Explor. 47, 63–89.

Peucker, T.K., Douglas, D.H., 1975. Detection of surface-specific points by local parallel processing of discrete terrain elevation data. Comput. Graphics Image Process. 4, 375–387.

Plant, J.A., Reeder, S., Salminen, R., Smith, D.B., Tarvainen, T., De Vivo, B., Petterson, M.G., 2003. The distribution of uranium over Europe: geological and environmental significance. Appl. Earth Sci. 112, B221–B238.

Plant, J.A., Whittaker, A., Demetriades, A., De Vivo, B., Lexa, J., 2005. The geological and tectonic framework of Europe. Chief Ed. In: Salminen, R., Batista, M.J., Bidovec, M., Demetriades, A., De Vivo, B., De Vos, W., Duris, M., Gilucis, A., Gregorauskiene, V., Halamic, J., Heitzmann, P., Lima, A., Jordan, G., Klaver, G., Klein, P., Lis, J., Locutura, J., Marsina, K., Mazreku, A., O'Connor, P.J., Olsson, S.Å., Ottesen, R.-T., Petersell, V., Plant, J.A., Reeder, S., Salpeteur, I., Sandström, H., Siewers, U., Steenfelt, A., Tarvainen, T. (Eds.), FOREGS – Geochemical Atlas of Europe. Part 1: Background, Information, Methodology and Maps. Geological Survey of Finland, Espoo, pp. 23–42. http://weppi.gtk.fi/publ/foregsatlas/articles/Geology.pdf.

Ramsey, M.H., 1998. Sampling as a source of measurement uncertainty: techniques for quantification and comparison with analytical sources. Anal. Atom. Spectrom. 13, 97–104.

Reimann, C., Demetriades, A., Eggen, O.A., Filzmoser, P., EuroGeoSurveys Geochemistry Group, 2009. The EuroGeoSurveys Geochemical Mapping of Agricultural and Grazing Land Soils Project (GEMAS) — evaluation of quality control results of aqua regia extraction analysis. In: NGU Report 2009.049. Geological Survey of Norway, Trondheim 94 pp. http://www.ngu.no/upload/Publikasjoner/Rapporter/2009/2009_049.pdf.

Reimann, C., Flem, B., Fabian, K., Birke, M., Ladenberger, A., Négrel, P., Demetriades, A., Hoogewerff, J., The GEMAS Project Team, 2012. Lead and lead isotopes in agricultural soils of Europe – the continental perspective. Appl. Geochem. 27, 532–542.

Reimann, C., Birke, M., Demetriades, A., Filzmoser, P., O'Connor, P. (Eds.), 2014. Chemistry of Europe's Agricultural Soils – Part A: Methodology and Interpretation of the GEMAS Data Set. Geologisches Jahrbuch (Reihe B 102) Schweizerbarth, Hannover 528 pp. http://www.schweizerbart.de/publications/detail/isbn/9783510968466.

Reimann, C., Birke, M., Demetriades, A., Filzmoser, P., O'Connor, P. (Eds.), 2014. Chemistry of Europe's Agricultural Soils – Part B: General Background Information and Further Analysis of the GEMAS Data Set. Geologisches Jahrbuch (Reihe B 103) Schweizerbarth, Hannover 352 pp. http://www.schweizerbart.de/publications/detail/isbn/9783510968473/Geologisches_Jahrbuch_Reihe_B_Heft_B103_Chemistry.

Reimann, C., Demetriades, A., Birke, M., Filzmoser, P., O'Connor, P., Halamić, J., Ladenberger, A., the GEMAS Project Team, 2014c. Distribution of elements/parameters in agricultural and grazing land soil of Europe. In: Reimann, C., Birke, M., Demetriades, A., Filzmoser, P., O'Connor, P. (Eds.), Chemistry of Europe's Agricultural Soils – Part A: Methodology and Interpretation of the GEMAS Data Set. Geologisches Jahrbuch (Reihe B102) Schweizerbarth, Hannover, pp. 103–474 (Chapter 11).

Salminen, R., Batista, M.J., Bidovec, M., Demetriades, A., De Vivo, B., De Vos, W., Duris, M., Gilucis, A., Gregorauskiene, V., Halamic, J., Heitzmann, P., Lima, A., Jordan, G., Klaver, G., Klein, P., Lis, J., Locutura, J., Marsina, K., Mazreku, A., O'Connor, P.J., Olsson, S.Å., Ottesen, R.-T., Petersell, V., Plant, J.A., Reeder, S., Salpeteur, I., Sandström, H., Siewers, U., Steenfelt, A., Tarvainen, T. (Eds.), 2005. FOREGS Geochemical Atlas of Europe, Part 1: Background Information, Methodology and Maps. Geological Survey of Finland, Espoo (Chief Ed.). 526 pp. http://weppi.gtk.fi/publ/foregsatlas/.

Scheib, A.J., Birke, M., Dinelli, E., Project Team, G.E.M.A.S., 2014. Geochemical evidence of aeolian deposits in European soils. Boreas 43 (1), 175–192.

Shahi, H., Ghavami, R., Rouhani, A.K., Kahoo, A.R., Haroni, H.A., 2015. Application of Fourier and wavelet approaches for identification of geochemical anomalies. J. Afr. Earth Sci. 106, 118–128.

Silverman, B.W., 1986. Density Estimation for Statistics and Data Analysis. Chapman and Hall, New York 176 pp. https://ned.ipac.caltech.edu/level5/March02/Silverman/Silver_contents.html.

Simpson, D.W., Anders, M.H., 1992. Tectonics and topography of the Western United States - an application of digital mapping. GSA Today 2, 118–121.

Sinclair, A.J., 1974. Selection of threshold values in geochemical data using probability graphs. J. Geochem. Explor. 3, 129–149.

Sinclair, A.J., 1976. Application of Probability Graphs in Mineral Exploration. Special Volume 4. Association of Exploration Geochemists, Toronto (95 pp).

Sinclair, A.J., 1983. Univaritate analysis. Chapter 3. In: Howarth, R.J. (Ed.), Statistics and Data Analysis in Geochemical Prospecting. Vol. 2 In: G.J.S. (Series Editor), Handbook of Exploration Geochemistry Elsevier, Amsterdam, pp. 59–81.

Sinclair, A.J., 1986. Statistical interpretation of soil geochemical data. In: Fletcher, W.K., Hoffman, S.J., Mehrtens, M.B., Sinclair, A.J., Thompson, I. (Eds.), Exploration Geochemistry: Design and Interpretation of Soil Surveys. Reviews in Economic Geology, Vol. 3, J.M. Robertson (Series Editor) Society of Economic Geologists, Chelsea, MI, USA, pp. 97–115.

Sinclair, A.J., 1991. A fundamental approach to threshold estimation in exploration geochemistry: probability plots revisited. J. Geochem. Explor. 41, 1–22.

Spielhagen, R.F., Baumann, K.-H., Erlenkeuser, H., Nowaczyk, N.R., Norgaard-Pedersen, N., Vogt, C., Weiel, D., 2004. Arctic Ocean deep-sea record of Northern Eurasian ice sheet history. Quat. Sci. Rev. 23 (11 – 13), 1455–1483.

Svendsen, J.I., Alexanderson, H., Astakhov, V.I., Demidov, I., Dowdeswell, J.A., Funder, S., Gataullin, V., Henriksen, M., Hjort, C., Houmark-Nielsen, M., Hubberten, H.W., Ingolfsson, O., Jacobsson, M., Kjaer, K., Larsen, E., Lokrantz, H., Lunkka, J.P., Lysa, A., Mangerud, J., Matioushkov, A., Murray, A., Möller, P., Niessen, F., Nikolskaya, O., Polyak, L., Saarnisto, M., Siegert, C., Siegert, M.J., Spielhagen, R.F., Stein, R., 2004. Late Quaternary ice sheet history of northern Eurasia. Quat. Sci. Rev. 23 (11), 1229–1272.

Takahashi, S., Ikeda, T., Shinagawa, Y., Kunii, T.L., Ueda, M., 1995. Algorithms for extracting correct critical points and constructing topological graphs from discrete geographical elevation data. Comput. Graphics Forum 14 (3), 181–192.

Tarvainen, T., Albanese, S., Birke, M., Ponavic, M., Reimann, C., The GEMAS Project Team, 2013. Arsenic in agricultural and grazing land soils of Europe. Appl. Geochem. 28, 2–10.

Tennant, C.B., White, M.L., 1959. Study of the distribution of some geochemical data. Econ. Geol. 54, 1281–1290.

Tukey, J.W., 1977. Exploratory Data Analysis. Addison-Wesley (506 pp).

Windley, B.F., 1984. The Evolving Continents. John Wiley & Sons, Chichester, England and New York (399 pp).

Xiao, F., Chen, J., Hou, W., Wang, Z., Zhou, Y., Erten, O., 2017. A spatially weighted singularity mapping method applied identify epithermal Ag and Pb-Zn polymetallic mineralization associated geochemical anomaly in Northwest Zhejiang, China. J. Geochem. Explor. http://dx.doi.org/10.1016/j.gexplo.2017.03.017.

Xie, S., Cheng, Q., Ke, X., 2008. Identification of geochemical anomaly by multifractal analysis. J. China Univ. Geosci. 19, 334–342.

Zhang, C., Jordan, G., Higgins, A., 2007. Using neighbourhood statistics and GIS to quantify and visualize spatial variation in geochemical variables: an example using Ni concentrations in the topsoils of Northern Ireland. Geoderma 137, 466–476.

Zuo, R., 2014. Identification of weak geochemical anomalies using robust neighborhood statistics coupled with GIS in covered areas. J. Geochem. Explor. 136, 93–101.

Zuo, R., Wang, J., 2016. Fractal/multifractal modeling of geochemical data: a review. J. Geochem. Explor. 164, 33–41.

Zuo, R., Wang, J., Chen, G., Yang, M., 2015. Identification of weak anomalies: a multifractal perspective. J. Geochem. Explor. 148, 12–24.